A quantitative inventory of yeast P body proteins reveals principles of compositional specificity

Wenmin Xing[1], Denise Muhlrad[2], Roy Parker[2], Michael K. Rosen[1]

[1]Department of Biophysics, Howard Hughes Medical Institute, UT Southwestern Medical Center, Dallas, TX, 79390

[2]Department of Biochemistry, Howard Hughes Medical Institute, University of Colorado, Boulder, CO, 80309

Corresponding author: michael.rosen@utsouthwestern.edu (M.K.R.)

ABSTRACT

P bodies are archetypal biomolecular condensates that concentrate proteins and RNA without a surrounding membrane. While dozens of P body proteins are known, the concentrations of components in the compartment have not been measured. We used live cell imaging to generate a quantitative inventory of the major proteins in yeast P bodies. Only 7 proteins are highly concentrated in P bodies (5.1-15 μM); the 24 others examined are appreciably lower (most ≤ 2.4 μM). P body concentration correlates inversely with cytoplasmic exchange rate. Sequence elements driving Dcp2 concentration into P bodies are distributed across the protein and act cooperatively. Strong correlation between interaction valency of components and P body concentration suggests how the composition of other condensates may be estimated from known interaction data. Our data indicate that P bodies, and probably other condensates, are biochemically simpler than suggested by proteomic analyses, with implications for specificity, reconstitution and evolution.

Currently 149 words (limit = 150)

INTRODUCTION

Eukaryotic cells contain numerous compartments that concentrate specific sets of molecules without a surrounding membrane (Banani et al., 2017; Shin and Brangwynne, 2017). These structures, referred to as biomolecular condensates, are related to a variety of biological processes. Examples include cytoplasmic processing bodies (P bodies) associated with RNA metabolism (Decker and Parker, 2012); promyelocytic leukemia nuclear bodies (PML NBs) involved in transcription, DNA damage repair, and anti-viral responses (Lallemand-Breitenbach and de Thé, 2010); signaling clusters in T cell activation (Su, 2016); and HP1 clusters in heterochromatin organization (Larson et al., 2017; Strom et al., 2017). While recent data indicate that condensates can have a variety of material properties and sometimes contain substructures (Banani et al., 2017; Shin and Brangwynne, 2017), significant portions of many condensates behave as dynamic liquids, showing fusion and fission, surface tension that makes them generally round, and rapid exchange of many components with the surrounding cytoplasm or nucleoplasm (Brangwynne et al., 2009, 2011; Dundr et al., 2004; Wang et al., 2014; Weidtkamp-Peters et al., 2008). These behaviors, and the sharp response of some condensates to concentration or temperature changes, suggest that liquid-liquid phase separation plays an important role in generating these compartments in cells (Brangwynne et al., 2009; Falahati and Wieschaus, 2017; Li et al., 2012; Riback et al., 2017; Saha et al., 2016; Smith et al., 2016). The activities of biomolecular condensates are thought to derive from the assembly of specific collections of functionally related molecules into a unique physical environment. Thus, understanding condensates as chemical entities requires knowledge and understanding of their compositions.

Large scale proteomics studies have been performed to determine comprehensive inventories of molecules that localize to different condensates, including stress granules (Jain et al., 2016; Markmiller et al., 2018; Youn et al., 2018), P bodies (Hubstenberger et al., 2017; Youn et al., 2018), and nucleoli (Anderson, 2002). There are also extensive studies on the localization of individual molecules to different condensates. Cumulatively, these studies generate partially overlapping lists of tens to hundreds of proteins and, in some recent work, RNA molecules in different condensates. Although some

transcriptomic studies and a few analyses of individual proteins have been quantitative (Khong et al., 2017; Klingauf et al., 2006; Leung et al., 2006; Wheeler et al., 2017), proteomic studies to date have been only qualitative. So both the relative and absolute concentrations of proteins in condensates are largely unknown, as are ways of predicting these features from existing data. Additionally, the relationships between concentration and dynamics of molecules in condensates have not been systematically explored.

We recently proposed a model to explain certain features of the compositions of biomolecular condensates (Banani et al., 2017; Ditlev et al., 2018). The model is based on distinctions between two classes of molecules: scaffolds and clients. Scaffolds are defined as condensate components that contribute to the assembly of the compartment. Thus, deletion of scaffolds decreases the size and/or numbers of condensates. In contrast, clients are not necessary for integrity of the structure, but are recruited by interacting with scaffolds. Scaffolds often have high valency of interaction elements and exhibit slow molecular dynamics, while clients often have lower valency and faster dynamics. Where studied, there are generally few scaffolds and many clients in natural condensates (Ditlev et al., 2018). Implicit in the model is that scaffolds should have higher concentration within the condensate than clients, since the former recruit the latter. The model was generated based on the behaviors of engineered multivalent macromolecules, where the distinction between scaffold and client was stark by design. In more complicated natural condensates, however, the distinction between scaffolds and clients may be more ambiguous, and could depend on expression levels and cell conditions (Ditlev et al., 2018). Nevertheless, initial features of the model were validated by the behaviors of several molecules in two natural condensates, PML NBs and yeast P bodies.

To examine the composition of a complex cellular condensate in a quantitative manner, we have performed a systematic analysis of yeast P bodies, an archetypical biomolecular condensate. P bodies are protein- and mRNA-rich cytoplasmic condensates conserved from yeast to mammals (Ingelfinger et al., 2002; Sheth and Parker, 2003; van Dijk et al, 2002). They are thought to participate in RNA metabolism, modulating mRNA decay and/or acting as sites of RNA storage during cellular stress (Aizer et al., 2014;

Bhattacharyya et al., 2006; Cougot et al., 2004; Sheth and Parker, 2003). Taking advantage of an available yeast GFP library, we used quantitative fluorescence microscopy to measure the absolute concentrations of 31 P body resident proteins within the condensates and in the surrounding cytoplasm. We also measured their dynamic properties using fluorescence recovery after photobleaching (FRAP). We find that P body proteins segregate into two groups based on their concentrations in P bodies and dynamics. Members of the first group (Dcp2, Edc3, Pat1, Xrn1, Lsm1, Dhh1, Upf1) are highly concentrated in P bodies (5.1-15 μM) and exchange slowly with the cytoplasm. All genetically-identified protein scaffolds of yeast P bodies are in this group. In contrast, members of the second group are substantially less concentrated in P bodies (all except Sbp1, 0.7-2.4 μM) and exhibit faster dynamics. These data are consistent with the scaffold-client model of condensate composition, and suggest that while a condensate may contain many components, only a small number are highly concentrated there. In a molecular dissection of Dcp2, we find that the N-terminal domain, multivalent C-terminal domain, and central high affinity Edc3 binding site all contribute to partitioning of the protein into P bodies and to its dynamic exchange with the cytoplasm. Moreover, the N-terminal and C-terminal domains can act cooperatively to promote recruitment of Dcp2 into P bodies. This highly distributive organization suggests a ready means of quantitatively modulating condensate composition during evolution. Surprisingly, a simplistic analysis of the known interactions of the major P body proteins reveals a strong correlation between the valency of partner binding and concentration in the compartment, suggesting that the composition of other biomolecular condensates may be predictable from known interaction data. We suggest that similar quantitative analyses will be important in understanding the assembly, compositions, and chemical and biological functions of other biomolecular condensates.

RESULTS

Strategies for quantification of P body proteins

In order to understand the chemical nature of a condensate it is important to both know its members, and also their concentrations. While recent experiments have generated multiple lists of the components of RNP granules, very little information is available on the

relative and absolute concentrations of these components in the compartments. Two criteria must be met to accurately measure protein concentrations in a condensate based on fluorescence intensities alone: 1) the size of the condensate must be larger than the point spread function (PSF, i.e. the diffraction limit) of the microscope used in the analysis since the fluorescence intensities are diluted for small objects (Fink et al., 1998); 2) the composition of the condensate cannot change over time, allowing reliable comparisons among multiple condensates in multiple cells. P bodies in wild type *S. cerevisiae* are typically diffraction-limited in size under normal conditions. But they become larger when mRNA decay is decreased, e.g. when mRNA decay proteins such as Dcp1 are deleted or when cells respond to stresses such as glucose starvation (Teixeira et al., 2005, 2007). Initially we analyzed GFP-tagged proteins expressed in a *dcp1Δ* strain, because the effects of stress are time-dependent and thus more difficult to systematically measure across a series of strains. We used confocal microscopy, limiting our analyses to P bodies that were larger than the x-y PSF of our microscope, and correcting for the diluting effect of the larger z-PSF based on an assumption that the structures were spherical.

Using this approach, we individually expressed 31 reported P body resident proteins tagged with GFP at their C-termini in their chromosomal location under their endogenous promoters in a *dcp1Δ* strain (Figure S1A, and Table S2). For each protein, we measured the absolute concentration in the P body and in the surrounding cytoplasm, based on cellular fluorescence intensity and independent calibration of fluorescence versus GFP concentration on our microscope. We calculated the partition coefficient (PC) as the ratio of these two values.

We also used fluorescence recovery after photobleaching (FRAP) to measure the exchange between P bodies and the cytoplasm. Of the 31 proteins, 19 showed sufficiently punctate distributions in mid-log phase to permit analysis (PC > ~2). We presume these puncta are P bodies because of previous reports that the proteins localize to P bodies and because in all cases tested we observed co-localization of the proteins with an mCherry-tagged P body marker, Edc3 (Figure S1B). We refer to these 19 proteins as regular P body proteins hereafter. The remaining 12 proteins were distributed relatively

uniformly in the cytoplasm and their P body concentrations could not be analyzed; these may be stress or strain specific proteins that do not concentrate in P bodies under our experimental conditions (Table S2).

Two observations suggest that the GFP tag probably does not strongly affect protein behaviors. First, the PC values and dynamics of Edc3 and Dhh1 tagged with GFP and mCherry were similar (Figure S2A and S2B). Second, the PC values and dynamics of Dcp2 are nearly identical with an N-terminal or C-terminal GFP tag (Figure S2C). In a screen of this size it is not practical to validate each protein with multiple tags at multiple locations, and it remains possible that some other proteins are affected by the tag.

Seven proteins/assemblies are highly concentrated in P bodies

We obtained PC for all 19 regular P body proteins, which revealed subclasses of these molecules. Average PC values of the 19 regular P body proteins had a wide range, with a maximum of 133 (Dcp2) steadily decreasing to a minimum of ~5 (Eap1, Ssd1) (Figure 1A). Only a few proteins had high partition coefficients, including Dcp2 (133 ± 13), Edc3 (133 ± 8) and Pat1 (107 ± 12); the majority had PC values <20. PC values of a given protein varied between 25 – 45% of the average, both among P bodies in a given cell and between cells, although the intracellular variation tended to be slightly smaller. With only 1 component labeled in each cell, it was not possible to assess correlations between PC values of different components (see discussion).

We also obtained absolute concentrations of each protein in P bodies, which ranged from ~0.7 μM to 15 μM and revealed two notable features of P bodies. First, seven proteins, Dcp2, Edc3, Pat1, Xrn1, Lsm1 (likely representing the entire, constitutive Lsm1-7 assembly (Sharif and Conti, 2013), Dhh1 and Upf1 – had average P body concentrations of 8.9 – 12 uM, with a slightly higher concentration (15 uM) for Dcp2 and slightly lower concentration (5 μM) for Upf1. We refer to these components as core P body proteins. A second striking observation was that there was a clear, sharp distinction between highly concentrated and more diffuse proteins (Figure 1B). After the core components most other proteins have P body concentrations < 2.5 uM, with most ~1 μM. The only

exceptions is Sbp1 (4.6 uM), which also has a very high cytoplasmic concentration, affording it a high P body concentration even with a small PC value (Figure 1, Table S1). Sbp1 also is not highly enriched in glucose-starved wild type P bodies (see below); for these reasons we do not include it in the core group, even though it has modestly high concentration in *dcp1Δ* P bodies. Thus, there is a large drop in P body concentration between the seven core proteins, and most other non-core proteins.

Two observations suggest that our data are consistent with previously reported measurements. First, the stoichiometry of protein complexes including Pat1/Lsm1 (1:1) and CCR4/Pop2(1:1) was the same as in previous biochemical characterizations (Basquin et al., 2012; Sharif and Conti, 2013). Upf1 concentrates in P bodies more than Upf2/Upf3 (which show 1:1 stoichiometry), consistent with previous findings that Ufp1 functions upstream, and independently of Upf2 and Upf3, which act as a constitutive complex (Sheth and Parker, 2006). Second, the total cellular concentrations that we measured are similar to a unified quantitative protein abundance database of *S. cerevisiae* (Ho et al., 2018) (Figure S2D).

By knowing the concentrations of 31 proteins in P bodies analyzed here, and their molecular weights, we were able to calculate the fractional contribution of the core components to the total protein mass of P bodies ($\sum_{core}(Ci * MWTi) / \sum_{All}(Ci * MWTi)$), where C_i and MWT_i are the P body concentration and molecular weight of the ith species, respectively). This estimate assumes conservatively that the 12 reported P body residents that lacked puncta in our analysis (Table S2) had the same concentration in P bodies as Psp2, the least concentrated component we could observe. It also neglects the (probably small) contributions of other proteins that might be in P bodies but were not analyzed here. By these calculations, the seven core proteins, including the whole Lsm1-7 complex, constitute approximately 83% of the total protein mass of P bodies (see Methods). Together, these data show that while yeast P bodies contain many different proteins, the majority of these are only weakly concentrated in the compartment, and a relatively small number make up the bulk of the structure.

Core proteins tend to have slow dynamics

We also examined the dynamics of the 19 regular P body proteins using FRAP. For each GFP-fusion expressing strain, entire P bodies (0.4 - 0.8 um) were photobleached and the fluorescence recovery curves were fit to single exponentials. The exponential rate constant of exchange (*k*) and extent of recovery were used to assess their dynamics. This analysis revealed that the regular P body proteins exchange with the cytoplasm with very different rates and fractional recoveries (Figure S3 and Table S1). At one end of the distribution, Dcp2 and Edc3 showed no measurable recovery on a 150 second timescale. Proteins such as Pat1 and Upf1, showed intermediate rates and extents of recovery (k = ~$0.01s^{-1}$, recovery = ~50%). While at the other end of the spectrum, proteins such as Sbp1 and Eap1 recovered nearly 100% in 150s (k =$0.07s^{-1}$) (Figure S3 and Table S1).

Since we observed heterogeneity of both partitioning and dynamics, we asked whether these parameters are related. For each protein, we plotted the exchange rate (*k)*, and extent of recovery against P body concentration (Figure 2A and 2B). Although exchange rate and recovery for both core proteins and non-core proteins spanned broad ranges, the core proteins (Dcp2, Edc3, Pat1, Xrn1, Lsm1, Upf1, and Dhh1) tended to have slower exchange rates and less fractional recovery than the non-core proteins (Figure 2A and 2B). On average, for the core group, the exchange rate was five-fold smaller than the non-core group, and recovery fraction was two-fold lower (Figure 2A and 2B).

Three observations argue that the slower recovery dynamics of the core proteins are not simply due to smaller fluorescent pools in cytoplasm, but rather reflect different interactions in the P body. First, neither exchange rate nor fractional recovery correlates with protein concentrations in cytoplasm (Figure S4A and S4B). Second, less than 50% of the total pool of each protein is localized to the P body (< 8% for most), suggesting that there are still substantial fluorescent pools in the cytoplasm (Figure 3). Third, we also performed inverse FRAP (iFRAP), which is insensitive to the size of fluorescent pools, for several proteins. In iFRAP, the entire cytoplasm except one P body was bleached and the loss of fluorescence in the P body was followed over time. In each case, the exchange rate and fractional recovery measured by iFRAP was similar to those measured by FRAP

(Figure S4C and S4D). Collectively, our data suggest the seven core P body proteins tend to exchange slowly with the surrounding cytoplasm, while non-core proteins tend to exchange more rapidly.

Partitioning and dynamics of proteins are not strongly affected by Dcp1 deletion

Since the above analysis was all performed in a *dcp1*Δ strain, we wanted to measure PC and P body dynamics under a different set of conditions to evaluate if the Dcp1 deletion made a substantial impact on P body composition or dynamics. For this experiment, we analyzed wild type strains after 30-60 min of glucose starvation, a stress that is known to promote P body assembly (Teixeira et al., 2005). By several criteria, we observed similar results to our analysis in *dcp1*Δ strains.

First, similar to the *dcp1*Δ strains, during glucose deprivation, Dcp2, Edc3, Pat1, Lsm1, Xrn1, Upf1, and Dhh1, remain the most concentrated proteins in wild type P bodies, although Pat1 and Lsm1 dropped somewhat compared to the *dcp1*Δ strains (Figure S5A and S5B). Two additional proteins also partition strongly into wild type P bodies under glucose starvation, Dcp1 and Pby1. Dcp1 binds with high affinity to Dcp2, and Pby1, in turn, binds strongly to Dcp1, explaining its absence in *dcp1Δ* P bodies (Krogan et al., 2006). In contrast to the core group, in these experiments only two members of the non-core group, Hek2 and Sbp1, partition sufficiently strongly into P bodies to permit analysis suggesting that the partitioning of low occupancy clients is lower under glucose starvation (see discussion).

We also observed that the dynamics of all proteins were qualitatively similar in glucose deprivation as compared to the *dcp1Δ* strains. The core proteins have slower dynamics, although there is no clear distinction between core and non-core concentrated groups because of limited number of the latter (Figure S5C and S5D). Nevertheless, these data suggest that partitioning and dynamics of proteins are qualitatively similar in the wild type strains under glucose starvation and the Dcp1 deletion strains, especially for the core proteins. We thus performed all subsequent experiments in *dcp1Δ* strains, unless stated otherwise.

P bodies do not strongly sequester their resident proteins

The biological importance of concentrating certain proteins into P bodies is unclear. One proposed function is that the P body could sequester molecules, inhibiting their activities in the cytoplasm. Similarly, P bodies have been suggested to store mRNAs or proteins under cellular stress, which could then be returned to the cytoplasm when the stress is resolved (Aizer et al., 2014; Bhattacharyya et al., 2006). To examine the efficiency of protein sequestration, we quantified the fractions of each P body protein in the compartments (F_P, the ratio of integrated fluorescence intensity within P bodies to the total fluorescence intensity in the entire cytoplasm), with the caveat that very small P bodies would likely be too dim to be observed (but see below). We first measured F_P in mid-log phase without stress. Under these conditions, the most concentrated proteins, Dcp2 and Edc3, are on average ~30% sequestered in observable P bodies (Figure 3). For the other highly concentrated proteins (Pat1, Xrn1, Lsm1, Upf1, and Dhh1), about 10% is sequestered in visible P bodies. The fraction in P bodies is even smaller for less concentrated proteins such that only about 5% of each is in visible P bodies.

We further asked if the degree of P body sequestration in *dcp1Δ* strains increases under glucose starvation (Teixeira and Parker, 2007). Thus, we measured F_P after 4h of glucose starvation. Although F_P increased for most of the proteins, visible P bodies still sequester less than 40% of each of the concentrated proteins (Figure S6A). We next grew cells to stationary phase to test if P bodies convert to sequestration sites at different growth stages. Again, less than 50% of each protein except Dcp2 and Edc3 is in P bodies (Figure S6B).

One possible explanation for the low degree of sequestration measured here is that many P bodies are too small to be observed by standard confocal microscopy. This would give artifactually low F_P values, as a significant fraction of P body-associated protein would not be accounted for in the integrated P body fluorescence intensity. Nevertheless, we can estimate an upper limit of F_P for most proteins by assuming that all P bodies in a given cell have identical compositions independent of size, and that the F_P value for the most

sequestered protein (Edc3), is, in fact 1 when small P bodies are properly accounted for. With this assumption, the estimated maximum F_P ($F_{P,max}$) for each protein would be $F_{P,max} = F_P * 1/ F_{P(Edc3)}$. Even with this conservative estimate, most proteins are only sequestered to < 20% in P bodies under all conditions.

Together, our quantitative measurements indicate that P bodies do not strongly sequester their resident proteins under the conditions examined here. This is because the volume of P bodies is very small compared to the total cytoplasmic volume (e.g. ~ 0.5% volume fraction in the *dcp1Δ* strains), so that even for a protein with a high PC value, most of the molecules are located in the surrounding cytoplasm rather than in the condensate. Our data are similar to other observations wherein only a small fraction of Argonaute protein accumulates in P bodies (Leung et al., 2006) and only ~18% of G3bp1 accumulates in mammalian stress granules (Wheeler et al., 2017). Our data of course do not rule out the possibility that sequestration could be higher under different conditions, nor do they speak to sequestration/storage of RNA, which could have even higher PC values than proteins, perhaps due to non-equilibrium processes (Ditlev et al., 2018; Hubstenberger et al., 2017).

Elements controlling Dcp2 partitioning and dynamics are distributed across the protein

We have shown that proteins concentrate into P bodies to different degrees and with distinct dynamic behaviors. We next sought to understand what molecular features could control these properties, using Dcp2 as an example, as one of the most highly concentrated and least dynamic P body components. We divided Dcp2 into three distinct regions (Figure 4A). The N-terminal domain (NTD) of the protein possesses decapping activity and binds to Dcp1 and mRNAs (Deshmukh et al., 2008). The multivalent C-terminal domain (CTD) contains multiple short helical leucine rich motifs (HLMs) that bind to Edc3. The analogous CTD of *S. pombe* Dcp2 phase separates with Edc3 through these multivalent interactions (Fromm et al., 2014). Finally, near the center of Dcp2, the first HLM (HLM1) appears to bind Edc3 with appreciably higher affinity than all other HLMs (Charenton et al., 2016), and mutations to this motif impair Dcp2 partitioning into P bodies (Harigaya et al., 2010). We expressed different Dcp2 mutants in *dcp1Δdcp2Δ* strains, in

which P bodies are still formed, as indicated by punctate Edc3 localization (Fig S7A), but they are smaller than in yeast expressing full length Dcp2, which is consistent with earlier results showing Dcp2 contributes to P body assembly (Teixeira and Parker, 2007). The analysis of these variants identified three molecular elements of Dcp2 that affect its partitioning into P bodies.

First, we found that N-terminally truncated Dcp2 (Dcp2 ΔN), which removes the RNA binding domain of the protein, partitions into P bodies less efficiently than the full-length protein (Dcp2 FL), with PC values of 72 ± 8 and 124 ± 9, respectively. FRAP analysis revealed that Dcp2 ΔN had an appreciably higher recovery fraction, 0.35 over 150 seconds, compared to Dcp2 FL, which does not recover at all in this timeframe (Figure 4B). This demonstrates that the N-terminal domain of Dcp2 promotes P body accumulation.

Second, mutating HLM1 (Dcp2 ΔH1) to alanine in the full length protein strongly decreased the PC to ~26, and increased the recovery after photobleaching to 0.65 over 150 seconds. Thus, both the NTD and HLM1 contribute to concentrating Dcp2 into P bodies and decreasing its exchange with the cytoplasm.

Third, truncation of the CTD (Dcp2 300) had no significant effect on the PC and dynamics of Dcp2 (Figure 4B). However, additional data suggest that the other HLMs in Dcp2's C-terminal extension can contribute to P body targeting when HLM1 is missing. Specifically, removing the C-terminal domain from Dcp2 ΔH1 (Dcp2 300 ΔH1) abolished its recruitment to P bodies (Figure 4C). Presumably, the C-terminal domain can contribute to Dcp2 partitioning in this context through the other HLMs interacting, albeit less effectively, with Edc3 (Fromm et al., 2014).

Since the N-terminal domain, HLM1, and C-terminal domain are all required for efficient partitioning and maintaining the characteristic slow dynamics of Dcp2, we conclude that elements controlling protein partitioning and dynamics are distributed across the protein.

RNA binding and turnover affect Dcp2 partitioning and dynamics

We further dissected the N-terminal region of Dcp2 and asked how interactions with RNA, an important scaffold of P bodies, affect partitioning and dynamics in *dcp1Δdcp2Δ* strains. Starting with the Dcp2 300 fragment, we either mutated previously reported RNA binding residues, R170, K212, K216, and R229, to alanine, or introduced repulsive interactions by mutating K212 and K216 to aspartate, generating Dcp2 300 AAAA, and Dcp2 300 ADDA, respectively (Figure 5A)(Deshmukh et al., 2008). PC values of both mutants decreased to ~85, from ~132 for wild type Dcp2 300 (Figure 5B), which is similar to the PC for the Dcp2ΔN construct which is missing the entire N-terminal domain (Figure 4B). Mutating the four RNA binding residues increased dynamics slightly, as both mutants recovered to 0.3 over 150 seconds (Figure 5C). These data suggest that binding to RNA enhances Dcp2 partitioning and maintains its slow dynamics of exchange.

To investigate the effect of catalytic activity on Dcp2 partitioning and dynamics, we made mutations in the Dcp2 ΔH1 construct, which affords a better dynamic range than the wild type protein (Figure 4B). We mutated W50 and D54, which were previously implicated in RNA cap recognition and hydrolysis, to alanine, giving Dcp2 ΔH1 WD (Figure 5A)(Charenton et al., 2016; Floor et al., 2010). In a *dcp1Δdcp2Δ* strain, this protein had PC values and dynamics similar to those of the parent Dcp2 ΔH1 (Figure S7B). One explanation for this behavior is that catalytic activity of Dcp2 is already low in the absence of Dcp1, so that subtle differences caused by mutations would not be observed. We thus analyzed Dcp2 ΔH1 and Dcp2 ΔH1 WD in a *dcp2Δ* strain, where the former protein should reconstitute significant mRNA decapping activity while the latter should not. Formation of P bodies was promoted by expressing Dcp2 ΔH1 WD (Figure 5D), which is consistent with mutations that block decapping catalysis leading to increased P bodies (Sheth and Parker, 2003; Teixeira and Parker, 2007). Dcp2 ΔH1 WD formed six P bodies per cell on average, compared to two P bodies per cell for Dcp2 ΔH1 (Figure 5E), despite being expressed at similar level (Figure S7C). More importantly, changing the catalytic rate of decapping changed the accumulation of Dcp2 in P bodies and altered its dynamics. Specifically, ~10% of Dcp2 ΔH1 WD was concentrated in visible P bodies compared with ~4% for Dcp2 ΔH1 (Figure 5E). The exchange rate also decreased from 0.041 s^{-1} to

$0.017s^{-1}$ and fractional recovery decreased from 0.85 to 0.65 in the WD mutant (Figure 5F). These data indicate that defective hydrolysis of the RNA cap promotes accumulation of Dcp2 in P bodies, and decreases Dcp2 dynamics. However, it is unclear whether the changes are caused by increasing amounts of cellular mRNA, which occurs when decapping is blocked, or by disrupting catalytic activity of Dcp2 *per se*.

Recruitment elements of Dcp2 act cooperatively

Different regions of Dcp2 contribute to partitioning into P bodies and modulate the dynamics of the protein. We next asked whether these regions can act cooperatively to promote P body recruitment. We analyzed three Dcp2 mutant fragments in *dcp1Δdcp2Δ* strains: 1) Dcp2 300 ΔH1, which lacks HLM1 and can only bind to RNA; 2) a C-terminal Dcp2 fragment where five out of ten HLMs have been inactivated by mutation, Dcp2C Δ5H, which binds Edc3 but not RNA; and 3) fusion of Dcp2 300 ΔH1 and Dcp2C Δ5H, Dcp2 ΔH1 Δ5H, which binds to both RNA and Edc3 (Figure 6A and 6D). The three mutants expressed at similar level in *dcp1Δdcp2Δ* strains (Figure S7C). We analyzed recruitment of the three proteins into P bodies using Edc3 as a marker for the compartments. Dcp2 300 ΔH1 and Dcp2C Δ5H are measurably recruited into microscopic P bodies in only ~20% and ~30% of cells, respectively. However, the fusion of the two fragments, Dcp2 ΔH1 Δ5H, is recruited into P bodies in ~95 % of cells (Figure 6B and Figure 6C). Moreover, partition coefficients of Dcp2 300 ΔH1 and Dcp2C Δ5H 2.5 and 3.5 respectively, while the partition coefficient of Dcp2 ΔH1 Δ5H is much higher, 31 (Figure 6D).

Thus, while Dcp2 300 ΔH1 and Dcp2C Δ5H are each recruited only weakly to P bodies, their fusion, Dcp2 ΔH1 Δ5H, is recruited strongly. This indicates that recruitment elements can act cooperatively when fused in cis, even when they recognize distinct ligands (in this case, Edc3 and RNA) within a condensate (Figure 6E).

Partitioning into P bodies correlates with interaction valency

Since Dcp2 fragments partition into P bodies stronger when binding to both Edc3 and RNA, we wondered whether proteins, in general, partition into condensates more

efficiently when they can interact with multiple molecules within the compartment. We summarized the number of identified protein-protein interacting elements and expected binding sites per mRNA molecule, expanding a previously published table (Rao and Parker, 2017) to include the 19 regular P body proteins in this study (Table S4). We only counted one valence if a protein interacts with multiple molecules through the same site. The total valency thus is an estimation of how many molecules one protein can interact with simultaneously. Surprisingly, given that our analysis did not include any information on binding affinity or avidity, the partition coefficients, P body concentrations, and fractional recovery values correlate strongly with total valency (Pearson r = 0.8) (Figure 7A, 7B and 7D). The highly concentrated proteins generally show multivalent interactions with each other and with less concentrated proteins, whereas the less concentrated proteins typically only interact with one, usually RNA, or two molecules. Protein dynamics, i.e. exchange rates, correlate with total valency to a lesser extent (Figure 7C).

Although there are some assumptions made in the correlative analysis (see comments for each protein, Table S4), our data suggest that multivalent interactions of highly concentrated proteins probably contribute to their higher partitioning and slower dynamics. This result suggests a way to predict the relative concentration of proteins, and the likelihood of a protein functioning as a scaffold or client, in other condensates based on known interaction data.

DISCUSSION

This work presents the first quantitative description of an RNP granule, which is representative of the broader class of non-membrane bound organelles referred to as biomolecular condensates. This analysis has revealed features of yeast P bodies that are generalizable to other condensates.

Distinctions between scaffolds and clients can explain compositions of natural biomolecular condensates.

Our work has revealed two clear classes of proteins within yeast P bodies, which exhibit the properties of scaffolds and clients as defined in our previous work (see Introduction)

(Banani et al., 2016). One class of proteins, which we name the core P body proteins, are a set of highly enriched proteins with PC ≥ 30 and P body concentrations > 5 μM, including Dcp2, Edc3, Pat1, the Lsm1-7 complex, Xrn1, Dhh1, and Upf1. On average, these proteins also show slower dynamics of exchange from P bodies and a small fraction of exchangeable molecules. Remarkably, the three most stable proteins within P bodies, Dcp2, Pat1, and Edc3, are the three major proteins shown to affect P body assembly (Buchan et al., 2008; Decker et al., 2007; Teixeira and Parker, 2007). Other core P body members also show multivalent interactions with each other (Rao and Parker, 2017; Swisher and Parker, 2011), and at least for Dhh1, Upf1, and the Lsm1-7 complex can contribute to P body assembly (Decker et al., 2007; Mugler et al., 2016; Sheth and Parker, 2006). These are properties predicted of scaffolds, which use multivalent interactions with multivalent partners to generate the network of contacts needed for condensate assembly. As a consequence of these interactions, scaffolds have increased partitioning into the condensate, and reduced exchange rates with the surrounding cytoplasm (Banani et al., 2016).

It is notable that in the *dcp1Δ* strains, the core components, Dcp2:Edc3:Pat1:Lsm1:Dhh1:Xrn1, are present at roughly equimolar concentrations (~10 μM), with the exception of Upf1, which is ~2-fold lower. In wild type yeast under glucose starvation, Pat1 and Lsm1 decrease ~2-fold together, becoming similar to Upf1. While these integral relationships may be fortuitous, it is also possible that P bodies are composed of discrete, equimolar complexes (e.g. Dcp2:Edc3:Dhh1:Xrn1 and/or Pat1:Lsm1-7) that assemble to higher order through additional interactions. Consistent with such a model, previous biochemical and cross-linking results have shown that the Pat1/Lsm1-7 co-complex binds the 3' end of deadenylated mRNAs and appears to be present at only one copy per mRNA (Chowdhury et al., 2007; Mitchell et al., 2013). Future studies where multiple proteins can be quantified at their native expression levels in individual cells will be necessary to examine this idea.

Our results identify a second set of proteins that show the behavior expected of condensate clients. Clients are defined as components that are not necessary for

formation of the condensate, but can be recruited into it through interactions with scaffolds. Clients show lower valency interactions with scaffolds and consequently lower partitioning into the condensate, and faster exchange rates as compared to scaffolds (exceptions would be clients with high affinity for scaffolds, which could concentrate more strongly and have slower exchange). The non-core components of P bodies behave as clients in that they show rapid exchange with the cytoplasm, and on average have appreciably lower PC values and P body concentrations. Since many of these are RNA binding proteins, we suggest they are recruited into P bodies by the high local concentration of RNA. Because they do not have additional protein-protein interactions with other core P body components, they show rapid exchange due to a presumed high rate of dissociation from RNA. Interestingly, the clients with the highest PC (Pop2, Ccr4, Upf2, Upf3) all also have direct interactions with a core P body component (Pop2 interacting with Dhh1, Upf2 interacting with Upf1), consistent with the idea that partitioning is determined by cooperative interactions of a given protein with multiple components within a condensate (see below).

Our results with P bodies demonstrate that condensates have discernable scaffolds and clients with distinct properties. Similar behaviors have been observed for other condensates as well. For example, the scaffold of PML NBs, the PML protein, exchanges with the nucleoplasm on a timescale of minutes, while the clients Sp100 and Daxx exchange in seconds (Weidtkamp-Peters et al., 2008). Analogously, the scaffold of the pericentriolar matrix in *C.elegans*, SPD-5, is stable and less dynamic, whereas the clients PLK-1, TPXL-1, SPD-2, and ZYG-9, are more mobile (Woodruff et al., 2017). Together, these data suggest that condensates may generally be organized around a relatively small number of highly concentrated, less dynamic scaffolds and large number of less concentrated, more dynamic clients. This construction would provide a relatively simple route for a condensate to appear during evolution, in that only a small number of proteins would need to develop the ability to assemble dynamically (either with themselves or with each other). Once this structure was established, other proteins could evolve the ability to interact with the scaffolds and consequently be recruited into the compartment (see also below). A composition of this nature also indicates that condensates are

biochemically less complicated than suggested by proteomics studies, where tens to hundreds of proteins have been annotated as residents of particular structures. Our quantitation indicates that most components are present in only small amounts, and the majority of the protein mass derives from only a few molecules. Such an understanding greatly simplifies efforts to reconstitute condensates *in vitro*, and can frame models of their biochemical functions.

Compositional specificity

A major question regarding biomolecular condensates is how the composition of the compartments is determined *in vivo*. Proteomic data and analyses of individual molecules have shown that condensates do have substantial specificity. While some components are shared between different compartments, many are uniquely concentrated in specific condensates. Simple mass action will concentrate clients that bind with high affinity to scaffolds. But many scaffolds interact with low specificity with many partners. For example, RNA binds relatively promiscuously with many RNA binding proteins, signaling modules (SH2, SH3, PDZ domains, etc.) often have broad specificity, and IDPs can weakly interact with many other IDPs. Since RNA, signaling domains and IDPs appear to be dominant components in various condensates, this promiscuity would degrade specificity of composition.

Our data on Dcp2 recruitment to P bodies suggests one means of solving this problem. We found that two fragments of Dcp2, which bind RNA and Edc3, respectively, partition only weakly into P bodies individually. Yet when fused together, they are recruited strongly. This behavior is analogous to previous observations that cooperativity between IDRs and folded domains can promote recruitment into both phase separated droplets *in vitro* and P bodies in cells (Lin et al., 2015; Protter et al., 2018). This suggests that in general, protein elements that bind scaffolds weakly, either specifically or non-specifically, will not partition strongly into a condensate. But when two such elements are fused together, even if they bind different scaffolds, they can be recruited strongly. This is analogous to, and in some cases may be mechanistically similar to, avidity effects in canonical molecular interactions, where high affinity can be achieved through multivalent

binding. Such effects will greatly narrow the specificity of recruitment, even for scaffolds that individually bind ligands promiscuously. This mechanism also provides ready routes for evolution of new clients through genetic rearrangements that fuse together multiple low-affinity interaction elements. Distributing recruitment across a large number of interaction elements would render composition less susceptible to mutations, which could lead to evolutionary selection. Therefore, partition into condensates through multiple binding elements may be evolutionarily favored to allow compositional specificity of biomolecular condensates.

Estimating composition and dynamics of biomolecular condensates through interaction data

Our analyses provide means to predict compositional and dynamic properties of other condensates that have not yet been analyzed quantitatively. We observed strong correlations of the concentration, PC and fractional recovery after photobleaching of P body components with the valency of interaction between components. In addition, we observed that all P body scaffolds are within the core group of components, while the non-core group contains exclusively clients. If these relationships hold generally, the relative valency of molecules within a condensate should allow prediction of the relative concentrations and dynamics of those molecules, and estimation of scaffolds and clients for the structure. The valency of direct interactions, in turn, can be determined from careful curation of low- (biochemical, yeast two-hybrid, etc.) and high-throughput (proteomic) interaction data for a condensate.

We emphasize that despite yielding strong correlations, our analysis here was extremely simplistic. Many factors beyond simply the number of non-exclusive binding partners may affect the partitioning and dynamics of components of biomolecular condensates. These include binding affinities, avidity effects, unknown interactions and active cellular processes. For example, clients with higher binding affinities for a scaffold should partition into condensates more strongly (Banani et al., 2016), and stronger binding between scaffolds should increase their partitioning (Wei et al., 2017). Enzymatic activities and mechanical forces exerted by ATP-consuming machines may alter protein dynamics and

partitioning. Thus, simple correlative analyses of valency should be viewed as a starting point to further explore the chemical and physical natures of biomolecular condensates.

Quantitative considerations of condensate function

Quantitative analyses as we have performed play an important role in assessing the functions of condensates. For example, several condensates, including P bodies, have been proposed as sites for sequestration/storage of biomolecules, in part because they appear as qualitatively bright puncta by microscopy, and in part because their disruption can activate certain processes (Arimoto et al., 2008; Decker and Parker, 2012; Li et al., 2000). However, as described above, when total condensate volume (typically < 1-2 % of cytoplasm/nucleoplasm even when accounting for sub-diffraction puncta, (Figure 3, Leung et al., 2006; Rao and Parker, 2017) and partition coefficients (2~200) are quantified, it is evident that only a small fraction of most molecular species are sequestered within condensates. While in some processes small changes in the amount of available species in the bulk cytoplasm/nucleoplasm could have functional consequences, in others, different mechanisms must be considered. For example, rather than sequestration, an inhibitory catalytic function within a condensate could also explain the activation of a process upon condensate disruption. Such considerations will further advance the already significant impact of biochemical reconstitutions of phase separation on understanding the functions of biomolecular condensates (Fromm et al., 2014; Schütz et al., 2017; Woodruff et al., 2017).

Conclusion

Our quantitative analyses have revealed that P bodies are compositionally simpler than previously envisioned, with only a small number of highly concentrated components. Among these are all of the genetically defined P body scaffolds. Rates of exchange between P bodies and the surrounding cytoplasm loosely correlate inversely with concentration within the compartment, although there are several exceptions, perhaps due to the influence of active processes. For a representative resident, Dcp2, concentration in the compartment results from the cooperative actions of multiple sequence elements. A surprisingly simple correlation between the valency of interactions

of a given protein with its concentration and dynamics in P bodies suggests a means of predicting the composition and properties of other biomolecular condensates. Available data suggest that these behaviors are likely general for other condensates and other condensate residents. Quantitative studies have important implications for the composition, function and evolution of biomolecular condensates.

FIGURE LEGENDS

Figure 1. Seven proteins are highly concentrated in P bodies

(A) Partition coefficients (PCs) of 19 P body proteins. Plots show PCs (black dots) and mean values (red line) ± standard error of the mean (SEM).

(B) Absolute concentrations in P bodies of 19 P body proteins. Plots show absolute concentrations in P bodies (black dots) and mean values (red line) ± SEM.

For (A) and (B) each dot represents an individual P body. One P body per cell was analyzed from 16 - 25 cells for each protein.

See also Table S1, Figure S1, Figure S2 and Figure S5.

Figure 2. Core proteins tend to have slow dynamics

Exchange rate (A) or fractional recovery (B) was plotted as a function of absolute concentrations in P bodies, respectively (mean ± SEM). Core and non-core proteins are indicated by red and black symbols, respectively. Graphs on the right show averaged exchange rate or fractional recovery (red lines) in core and non-core groups. Analysis of significance was calculated by Wilcoxon rank-sum test. *** and **** indicate p values less than 0.001 and 0.0005, respectively.

See also Table S1, Figure S2, Figure S3, Figure S4, and Figure S5.

Figure 3. P bodies do not strongly sequester their resident proteins

Plots show fractions in visible P bodies (black dots) and mean values (red lines) ± SEM in mid-log phase without any cellular stress. Each dot represents fraction of protein in visible P bodies corresponding to an individual cell. 16 - 25 cells were analyzed for each

protein. Similar fractions were observed under glucose starvation or in stationary phase (Figure S6).

Figure 4. Elements controlling Dcp2 partitioning and dynamics are distributed across the protein

(A) Schematics of domain architecture of Dcp2 FL and mutants. Red, N-terminal domain (NTD). Orange, HLM1. Blue, other 10 HLMs in C-terminal domain. Grey, inactivated HLMs.

(B) Partition coefficients and dynamics of GFP tagged Dcp2 FL, Dcp2 ΔN, Dcp2 ΔH1, and Dcp2 300 ΔH1 in *dcp1Δdcp2Δ* strain. Left plot shows PCs of Dcp2 FL (black), Dcp2 ΔN (red), and Dcp2 ΔH1 (orange), and mean values (bold horizontal bars) ± SEM. One P body per cell was analyzed from 19 cells. Right graph shows recovery curve as an average of 19 P bodies ± SEM. Significance was calculated by the Wilcoxon rank-sum test. *** and **** indicate p values less than 0.001 and 0.0005, respectively.

(C) Representative images of a *dcp1Δdcp2Δ* yeast strain expressing GFP tagged Dcp2 ΔH1 (left) and Dcp2 300 ΔH1 (right). Scale bar, 5um.

Figure 5. RNA binding and turnover affect Dcp2 partitioning and dynamics

(A) Schematics of domain architecture of Dcp2 300, Dcp2 300 AAAA, Dcp2 300 ADDA, Dcp2 ΔH1 and Dcp2 ΔH1 WD.

(B) PCs of Dcp2 300 (black), Dcp2 300 AAAA (magenta), and Dcp2 300 ADDA (green), and mean values (bold horizontal bars) ± SEM. One P body per cell was analyzed from 20 cells for Dcp2 300, and 40 cells for Dcp2 300 AAAA and Dcp2 300 ADDA. Significance was calculated by the Wilcoxon rank-sum test. ****, $p < 0.0005$.

(C) FRAP recovery curves (average of 20 or 40 P bodies ± SD) for Dcp2 300 and Dcp2 AAAA (left) or Dcp2 ADDA (right).

(D) Representative images of *Δdcp2Δ* yeast strain expressing GFP tagged Dcp2 ΔH1 and Dcp2 ΔH1 WD. Scale bar, 5um.

(E) Number of P bodies formed per cell. More than 300 cells expressing either Dcp2 ΔH1 (red) and Dcp2 ΔH1 WD (blue) were quantified.

(F) Total fractions of Dcp2 ΔH1 (red) and Dcp2 ΔH1 WD (blue) in P bodies. Plot shows averages of 35 P bodies ± SEM for Dcp2 ΔH1 and 37 P bodies ± SEM for Dcp2 ΔH1 WD. Significance was calculated by the Wilcoxon rank-sum test. ****, $p < 0.0005$

(G) Inhibition of RNA turnover slows Dcp2 ΔH1 exchange rate. Dcp2 ΔH1 WD recovered slower than Dcp2 ΔH1. Figures show FRAP recovery curves (average of 35 or 37 P bodies ± SD) of Dcp2 ΔH1 (red) and Dcp2 ΔH1 WD (blue).

See also Figure S7.

Figure 6. Distributed elements contribute to specific recruitment to biomolecular condensates

(A) Domain architecture of Dcp2 300 ΔH1, Dcp2C Δ5H and Dcp2 ΔH1 Δ5H.

(B) Representative images showing *dcp1Δdcp2Δ* yeast strains expressing GFP tagged Dcp2 300 ΔH1, Dcp2C Δ5H and Dcp2 ΔH1 Δ5H. Edc3-mCherry was also expressed as a P body marker. Scale bar, 5um.

(C) Fractions of cells exhibiting puncta formed by each mutant. n(Dcp2 300 ΔH1) = 163, n(Dcp2C Δ5H) = 188, n(Dcp2 ΔH1 Δ5H) = 204.

(D) Partition coefficients of GFP-tagged Dcp2 300 ΔH1, Dcp2C Δ5H and Dcp2 ΔH1 Δ5H, and mean values (red bold horizontal bars) ± SEM. 100 P bodies were analyzed. Significance was calculated by the Wilcoxon rank-sum test. **** indicates p values less than 0.0005.

(E) Specific recruitment to P bodies can be achieved by distributing elements across Dcp2.

See also Figure S7.

Figure 7. Proteins having multiple binding partners tend to partition into P bodies strongly

Partition coefficient (A), absolute concentrations in P bodies (B), exchange rate after photobleaching (C), and fractional recovery after photobleaching (D) were plotted as functions of total valency of each regular P body protein (mean ± SEM). Core and non-

core proteins are marked by red and black, respectively. Pearson correlation coefficients were calculated using Prism.

See also Table S4.

SUPPLEMENTARY FIGURE LEGENDS

Figure S1. Punctate localization of GFP tagged proteins and co-localization with P body marker, related to Figure 1.

(A) Confocal fluorescence microscopy images of 31 P body proteins fused to GFP expressed in yeast growing in log-phase. Scale bar, 5um (B) Fluorescence microscopy images of yeast co-expressing Edc3-mCherry and selected GFP-fused P body proteins. Scale bar, 5um.

Figure S2. Verification of quantitative measurements, related to Figures 1 and 2.

(A) A C-terminal GFP tag does not affect protein partitioning into P bodies. Partition coefficients of Edc3 and Dhh1 tagged at their C-termini with either GFP or mCherry. Plots show PC values (black dots) and means (red line) ± SEM. Each dot represents an individual P body in one cell. Significance was calculated using the Wilcoxon rank-sum test.

(B) A C-terminal GFP tag does not affect protein dynamics. Recovery curve of C-terminal GFP- or mCherry-tagged Edc3 and Dhh1 as an average of 20 P bodies ± SD.

(C) Location of the GFP tag does not affect partitioning or dynamics of Dcp2. Dcp2 was tagged with GFP at either its N- (N-GFP-Dcp2) or C-terminus (Dcp2-GFP). Top: PC (black dots) and mean values (red line) ± SEM. Significance was calculated using the Wilcoxon rank-sum test. Bottom: recovery curve as an average of 20 P bodies ± SD. (D) Comparison of protein abundance (molecules per cell) measured in this study to previous unified database (Ho et al., 2018).

Figure S3. FRAP recovery curves of 19 P body proteins, related to Figure 2.

FRAP recovery curves of 19 P body proteins reported as average of 16 - 25 P bodies ± SD.

Figure S4. Slow dynamics are not caused by smaller fluorescence pool in cytoplasm, related to Figure 2

(A/B) Exchange rate (A) or fractional recovery (B) is not correlated with protein concentrations in the cytoplasm. Exchange rate or fractional recovery (mean ± SEM) were plotted as a function of absolute concentrations in cytoplasm (mean ± SEM), respectively. P body core and non-core proteins are indicated by red and black symbols, respectively.

(C/D) Exchange rate (C) or fractional decay (D) measured by iFRAP are qualitatively similar to values measured using FRAP. The fractional decay of more rapidly exchanging proteins measured by iFRAP is systematically smaller than measured using FRAP due to the longer time to bleach the whole cytoplasm in the former experiments. P body core and non-core proteins are indicated by red and black symbols, respectively.

Figure S5. Partitioning and dynamics of P body proteins in wild type strains under glucose starvation are qualitatively similar to *dcp1Δ* strains, related to Figure 1 and Figure 2.

(A/B) Partition coefficients (A) and absolute concentrations (B) in P bodies in wild type strains under 30-60 min of glucose starvation. Plots show PC values, and absolute concentrations in P bodies (black dots) and mean values (red line) ± SEM. Each dot represents an individual P body in one cell. We analyzed 20 - 30 cells for each protein. Left, proteins found in both wild type and *dcp1Δ* strains ordered by their PC in *dcp1Δ* strains. Right, proteins only found in P bodies in wild type strains.

(C/D) Exchange rate (C) or fractional recovery (D) was plotted as a function of absolute concentration in P bodies (mean ± SEM). P body core and non-core proteins are indicated by red and black symbols, respectively.

Figure S6. P bodies do not strongly sequester their resident proteins, related to Figure 3.

(A) Fraction of total protein localized to P bodies (black dots) and mean values (red lines) ± SEM in *dcp1Δ* strains in mid-log phase under 4h glucose starvation.

(B) Fraction of total protein localized to P bodies (black dots) and mean values (red lines) ± SEM in *dcp1Δ* strains in stationary phase. In A and B, each dot corresponds to an individual cell, and twenty cells were analyzed for each protein.

Figure S7. related to Figure 4, Figure 5 and Figure 6.

(A) Representative images of *dcp1*Δ*dcp2*Δ yeast expressing Edc3-mCherry as a P body marker. Scale bar, 5um. (B) Mutations that impair RNA cap hydrolysis have no effect on Dcp2 partitioning or dynamics in *dcp1*Δ*dcp2*Δ yeast. Left plot shows distributions of PC values of Dcp2 ΔH1 (orange) and Dcp2 ΔH1 WD (purple), and mean values (bold horizontal bars) ± SEM. One P body per cell was analyzed from 20 cells. Significance was calculated using the Wilcoxon rank-sum test. Right graph shows recovery curve as an average of 20 P bodies ± SEM.

(C) Dcp2 mutants express at similar levels. Western blot of Dcp2 ΔH1 and Dcp2 ΔH1 WD in *dcp2*Δ yeast (left), and Dcp2 300 ΔH1, Dcp2C Δ5H and Dcp2 ΔH1 Δ5H expression in *dcp1*Δ*dcp2*Δ yeast (right).

METHODS

Yeast strains

Yeast strains used in this study are listed in Table S2. Yeast strains carrying plasmids were constructed using lithium acetate-based transformation (Gietz and Schiestl, 2007).

Plasmid construction

Plasmids used in this study are listed in Table S3. All Dcp2 mutants were expressed under the *DCP2* promoter on a low-copy centromeric plasmid (pRP1902) as previously reported (Harigaya et al., 2010). Dcp2 point mutations were made by site-directed mutagenesis using KOD Xtrem Hot start DNA Polymerase followed by Dpn1 digestion. Dcp2C Δ5H, and Dcp2 ΔH1 Δ5H were constructed by Gibson assembly into the vector used for Dcp2 FL, pRP1903 (Harigaya et al., 2010). N-Dcp2 was also constructed from pRP1903.

Yeast growth conditions

dcp1Δdcp2Δ strains and *dcp2Δ* strains expressing GFP-Dcp2 mutants were grown in synthetic medium lacking uracil but containing 2% glucose. *dcp1Δdcp2Δ* strains expressing both GFP-Dcp2 mutants and Edc3-mCherry were grown in the same media also lacking lysine. Glucose starvation in Figures S5 and S6 was performed by exchanging with the corresponding synthetic medium lacking 2% glucose for durations indicated in the text. Stationary stage in Figure S6 was achieved by growing cells for 5 days and OD_{600} > 6. For imaging, cells were grown at 30 °C until OD_{600} = 0.4 ~ 0.6, and then immobilized on concanavalin-A (Sigma-Aldrich) coated glass bottom dishes (MatTek).

Image acquisition and analysis

All images were acquired using a Leica SP8 Laser Scanning Confocal Microscope using a 100 X 1.4 NA oil immersion objective and photomultiplier tube (PMT) detector. Images were analyzed using Fiji.

Identification of P bodies

For strains expressing only GFP tagged protein, P bodies were identified by thresholding the GFP fluorescence intensity using the MaxEntropy algorithm in Fiji. For stains expressing both GFP tagged proteins and Edc3-mCherry in Figure 6, Edc3-mCherry signals were thresholded (MaxEntropy) to identify P bodies, and created masks. Partitioning of the Dcp2 mutants was assessed by the ratio of average GFP intensity within in the mask (P body identified by Edc3-mCherry signal) to the intensity outside the mask (cytoplasm). Positive GFP puncta were determined when the ratio is greater than 1.5. Because the formation of and partitioning into biomolecular condensates are sensitive to protein expression levels, we eliminated cells with low expression (bottom 10% of the populations) and high expression (top 10% in the populations) of GFP and mCherry.

Measurements of absolute concentrations in P bodies and cytoplasm, and partition coefficients

To quantify the absolute concentrations of GFP-tagged proteins in P bodies, we assume that P bodies are spherical (based on the similar diameters in x and y when measured), and correct their measured intensities based on the point spread function (PSF) of our microscope (Fink et al., 1998). We determined the PSF using 200 nm fluorescent microspheres (Invitrogen) imaged with the same optics, filters, zoom settings and pinhole settings used throughout our study. We then modeled (Matlab) the intensity-diluting effect of the PSF when imaging spheres of different sizes through convoluting the PSF with the sphere. This yielded a correction curve relating sphere diameter to the fraction of true maximum intensity actually measured in the image (Fink et al., 1998), assuming all fluorescence intensity derived from the sphere and none derived from the surroundings. We limited our cellular analyses to P bodies with measured diameter > 330 nm (most are 400-800 nm in *dcp1Δ* strains), which is 1.1 times larger than the x-y PSF, and thus can be accurately measured as the full width at half maximum intensity (FWHM) of the object. From the measured diameter in the x-y dimension, an assumption of spherical shape, and the correction curve, we determined the calibration factor (CF) for the P body intensity. To determine P body intensity ($I_{Pbody,measured}$), we first measured the maximum intensity of P body and then drew a one pixel circle around it to find the surrounding pixels. 9 pixels including the maximal one were averaged to get the $I_{Pbody,measured}$. Since the correction was based on the assumption that all fluorescence intensity derived from the object, we applied it only to the incremental intensity of the P body over the cytoplasm ($I_{Pbody,measured}$-I_{cyto}); cytoplasmic intensity also contributes to $I_{Pbody,\ measured}$, but is homogenous across the cell and should not be corrected for the PSF effect. The real maximum intensity of P body(I_{Pbody}) was thus calculated as [($I_{Pbody,measured}$-I_{cyto})/CF + I_{cyto}]. Cytoplasm intensity was calculated by averaging the mean intensities of three ROIs the same size as P bodies in the cytoplasm.

We used standard curves of the fluorescence intensities of GFP solutions imaged with identical parameters as yeast to convert I_{Pbody} and I_{cyto} to absolute concentrations in P bodies (C_{Pbody}) and the cytoplasm (C_{cyto}). Because the intensities of P bodies marked by different proteins have a large dynamic range, to avoid saturation of our camera, we

imaged them using different laser powers and gain settings, and generated different GFP standard curves accordingly. Partition coefficients were calculated as C_{Pbody}/C_{cyto}.

Fraction of protein mass in P bodies attributable to the core proteins

The core P body proteins are Dcp2, Edc3, Pat1, Xrn1, the Lsm1-7 complex, Upf1, and Dhh1. We assumed that the 12 reported P body proteins that lacked clear punctate localization in our studies here (Table S2) have the same P body concentrations as the least concentrated regular protein, Psp2 (Table S1). The mass of the ith protein in P bodies was calculated as the absolute P body concentration (C_i) multiplied by the molecular weight (MWT_i). The fraction of protein mass of the core proteins was determined by $\sum_{core}(Ci * MWTi)/\sum_{All}(Ci * MWTi)$, where *All* refers to the 31 reported P body proteins listed in Table S1.

Total fractions in P bodies and number of molecules per cell

We collected z-stacks of yeast cells with a 0.22 μm step size. To calculate the number of molecules in cytoplasm (N_{cyto}), we first measured the cell volume. Diameters in x, y and z directions were measured manually with Otsu thresholding to determine the cell boundaries in Fiji. Cell volume was calculated as $V_{cell} = 4/3*\pi*(x/2)*(y/x)*(z/2)$, assuming that yeast cells are ellipsoidal. Previous studies have shown that the cytoplasmic volume of a yeast cell is about 67% of the total cell volume (Uchida et al., 2011; Yamaguchi et al., 2011). To calculate the number of molecules in P bodies (N_{Pbody}), we measured the x-y diameter of each P body in the cell and calculated its volume by assuming a spherical shape. The concentrations in the cytoplasm (C_{cyto}) and P body (C_{Pbody}) were determined as described above. N_{cyto} and N_{Pbody} were calculated as $N_{cyto} = V_{cell} \times 0.67 \times C_{cyto} \times N_A$ (6.02×10^{23}). $N_{Pbody} = V_{Pbody} \times C_{Pbody} \times N_A$ (6.02×10^{23}). The fraction of molecules in P bodies is thus $N_{Pbody}/(N_{cyto} + N_{Pbody})$.

Fluorescence recovery after photobleaching (FRAP)

Selected P bodies were bleached using an 0.5W 488 nm laser at 60% laser power. Images were collected from a single plane using a 2.5 airy unit pinhole at 5 s intervals for 150 s. Fluorescence intensities were analyzed manually in Fiji. Background intensities

($I_{background}$) were first subtracted. Because yeast cells are small, the cytoplasm may be bleached slightly while bleaching the P bodies. We thus measured the average fluorescence intensities of cytoplasm (excluding the bleached P body) before bleaching ($I_{cytobefore}$) and in the first frame after bleaching ($I_{cytoafter}$) to account for this effect. An unbleached P body was used to correct for the photo-bleaching during image acquisition in the recovery phase ($I_{unbleached}$). The corrected recovered intensities ($I_{recovery}$) were normalized to the intensities pre-bleaching ($I_{pre\text{-}bleaching}$).

$$I_{recovery} = \frac{(I - I_{background})}{(I_{unbleached} - I_{background})} \times \frac{(I_{cytoafter} - I_{background})}{(I_{cytobefore} - I_{background})}$$

$$I_t = \frac{I_{recovery}}{(I_{pre-bleaching} - I_{background})}$$

Normalized intensities were fitted to a single exponential recovery (one-phase association function in Prism) (GraphPad Software).

$$I_{(t)} = I_\infty + (I_0 - I_\infty)e^{-kt}$$

where I_0 , I_∞ and *k* were fit as intensity immediately after bleach, intensity at long times and the rate constant for recovery, respectively. The fractional recovery was calculated as:

$$F = \frac{I_\infty - I_0}{1 - I_0}$$

inverse FRAP (iFRAP)

For iFRAP, the whole cytoplasm except one P body was bleached 3 times for a total of 1.5 s using a 0.5W 488 nm laser at 100% laser power. Fluorescence intensities were analyzed as in the FRAP experiments above. Because intensities of the unbleached P body were likely affected during bleaching, we normalized the intensity to the intensities of P body in the first frame after photo-bleaching (I_{pre}).

$$I_t = \frac{(I - I_{background})}{(I_{unbleached} - I_{background})} \times \frac{1}{(I_{pre} - I_{background})}$$

Normalized intensities were fitted to a single exponential decay (one-phase decay function in Prism) (GraphPad Software).

$$I_{(t)} = I_\infty + (I_0 - I_\infty)e^{-kt}$$

where I_0 , I_∞ and *k* were fitted parameters. The fractional decay was calculated as:

$$F = I_0 - I_\infty$$

Western blot

Yeast total extracts were prepared as previously described (Knop et al., 1999). 1.5 x 10^8 cells from OD_{600} = 0.4 – 0.6 cultures were resuspended in 1150 µl lysis buffer (0.24 M NaOH, 1% β-mercaptoethanol, 1 mM EDTA, 1 mM PMSF, 5 uM Pepstatin A, 10 uM Leupeptin). After incubation on ice for 20 min, 150 µl 55% trichloroacetic acid (TCA) was added to precipitate proteins on ice for 20 min. The mixture was centrifuged at 16100rpm at 4 °C for 10 min. The pellet was resuspened in 250 µl HU buffer (8 M urea, 5% SDS, 200 mM Tris-HCl [pH 6.8], 1 mM EDTA, 5% β-mercaptoethanol, and 1% bromophenol blue) and incubated at 65 °C for 10 min, followed by 16100rpm centrifugation at RT for 5 min. The supernatant was used for subsequent analyses. Immunoblotting was performed with primary antibodies: rabbit-anti-GFP (1:2000) (Abcam), and mouse-anti-PGK1 (1:1000) (Abcam). Mouse-anti-rabbit-IgG (1:10,000) (Santa Cruz) and goat-anti-mouse-IgG (1:10,000) (Santa Cruz) were used as secondary antibodies.

Quantifications and Statistical Analysis

Detailed statistics including number of cells analyzed, mean value, standard deviation and standard error of the mean are indicated in each figure legend. The Wilcoxon rank-sum test was performed using GraphPad Prism (GraphPad software). Significance was determined as: ***, $p < 0.001$; ****, $p < 0.0005$.

Acknowledgements

We thank Saumya Jain for discussions on performing FRAP; Salman Banani, Jon Ditlev and Allyson Rice for helpful discussions on image analysis; Simon Currie and Jon Ditlev for critical reading of the manuscript; and members of the Rosen lab for helpful discussions. This work was supported by the Howard Hughes Medical Institute (M.K.R. and R.P.) and Welch Foundation (grant I-1544, M.K.R.).

References

Aizer, A., Kalo, A., Kafri, P., Shraga, A., Ben-Yishay, R., Jacob, A., Kinor, N., and Shav-Tal, Y. (2014). Quantifying mRNA targeting to P bodies in living human cells reveals their dual role in mRNA decay and storage. J Cell Sci *127*, 4443-4456.

Anderson, J.S., Lyon, C.E., Fox, A.H., Leung, A.K.L., Lam, Y. W., Steen, H., Mann, M., Lamond, A. (2002). Directed Proteomic Analysis of the Human Nucleolus. Curr Biol *12*, 1-11.

Arimoto, K., Fukuda, H., Imajoh-Ohmi, S., Saito, H., and Takekawa, M. (2008). Formation of stress granules inhibits apoptosis by suppressing stress-responsive MAPK pathways. Nat Cell Biol *10*, 1324-1332.

Banani, S.F., Rice, A.M., Peeples, W.B., Lin, Y., Jain, S., Parker, R., and Rosen, M.K. (2016). Compositional Control of Phase-Separated Cellular Bodies. Cell *166*, 651-663.

Banani, S.F., Lee, H.O., Hyman, A.A., and Rosen, M.K. (2017). Biomolecular condensates: organizers of cellular biochemistry. Nat Rev Mol Cell Biol *18*, 285-298.

Basquin, J., Roudko, V.V., Rode, M., Basquin, C., Seraphin, B., and Conti, E. (2012). Architecture of the nuclease module of the yeast Ccr4-not complex: the Not1-Caf1-Ccr4 interaction. Mol Cell *48*, 207-218.

Bhattacharyya, S.N., Habermacher, R., Martine, U., Closs, E.I., and Filipowicz, W. (2006). Relief of microRNA-mediated translational repression in human cells subjected to stress. Cell *125*, 1111-1124.

Blewett, N.H., and Goldstrohm, A.C. (2012). A eukaryotic translation initiation factor 4E-binding protein promotes mRNA decapping and is required for PUF repression. Mol Cell Biol *32*, 4181-4194.

Brangwynne, C.P., Eckmann, C.R.M, Courson, D.S., Rybarska, A., Hoege, C., Gharakhani, J., Jülicher, F., Hyman, A.A. (2009). Germline P Granules Are Liquid Droplets That Localize by Controlled Dissolution/Condensation. Science *324*, 1729-1732.

Brangwynne, C.P., Mitchison, T.J., and Hyman, A.A. (2011). Active liquid-like behavior of nucleoli determines their size and shape in Xenopus laevis oocytes. Proc Natl Acad Sci U S A *108*, 4334-4339.

Buchan, J.R., Muhlrad, D., and Parker, R. (2008). P bodies promote stress granule assembly in *Saccharomyces cerevisiae*. J Cell Biol, *183*, 441–455.

Charenton, C., Taverniti, V., Gaudon-Plesse, C., Back, R., Seraphin, B., and Graille, M. (2016). Structure of the active form of Dcp1-Dcp2 decapping enzyme bound to m(7)GDP and its Edc3 activator. Nat Struct Mol Biol *23*, 982-986.

Charenton, C., Taverniti, V., Gaudon-Plesse, C., Back, R., Seraphin, B., and Graille, M. (2016). Structure of the active form of Dcp1-Dcp2 decapping enzyme bound to m(7)GDP and its Edc3 activator. Nat Struct Mol Biol *23*, 982-986.

Chowdhury, A., Mukhopadhyay, J., and Tharun, S. (2007). The decapping activator Lsm1p-7p-Pat1p complex has the intrinsic ability to distinguish between oligoadenylated and polyadenylated RNAs. RNA *13*, 998-1016.

Coller, J. M., Tucker, M., Sheth, U., Valencia-Sanchez, M. A., & Parker, R. (2001). The DEAD box helicase, Dhh1p, functions in mRNA decapping and interacts with both the decapping and deadenylase complexes. RNA *7*, 1717–1727.

Cougot, N., Babajko, S., and Seraphin, B. (2004). Cytoplasmic foci are sites of mRNA decay in human cells. J Cell Biol *165*, 31-40.

Decker, C.J., Teixeira, D., and Parker, R. (2007). Edc3p and a glutamine/asparagine-rich domain of Lsm4p function in processing body assembly in Saccharomyces cerevisiae. J Cell Biol *179*, 437-449.

Decker, C.J., and Parker, R. (2012). P bodies and stress granules: possible roles in the control of translation and mRNA degradation. Cold Spring Harb Perspect Biol *4*, a012286.

Deshmukh, M.V., Jones, B.N., Quang-Dang, D.U., Flinders, J., Floor, S.N., Kim, C., Jemielity, J., Kalek, M., Darzynkiewicz, E., and Gross, J.D. (2008). mRNA decapping is promoted by an RNA-binding channel in Dcp2. Mol Cell *29*, 324-336.

Ditlev, J.A., Case, L.B., and Rosen, M.K. (2018). Who's in and Who's Out-Compositional Control of Biomolecular Condensates. J Mol Biol.

Dunckley, T., Tucker, M., and Parker, R. (2001). Two related proteins, Edc1p and Edc2p, stimulate mRNA decapping in Saccharomyces cerevisiae. Genetics *157*, 27–37.

Dundr, M., Hebert, M.D., Karpova, T.S., Stanek, D., Xu, H., Shpargel, K.B., Meier, U.T., Neugebauer, K.M., Matera, A.G., and Misteli, T. (2004). In vivo kinetics of Cajal body components. J Cell Biol *164*, 831-842.

Falahati, H., and Wieschaus, E. (2017). Independent active and thermodynamic processes govern the nucleolus assembly in vivo. Proc Natl Acad Sci U S A *114*, 1335-1340.

Fink, C., Morgan, F., Loew, L.M. (1998). Intracellular Fluorescent Probe Concentrations by Confocal Microscopy. Biophys J *75*, 1648-1658.

Floor, S.N., Jones, B.N., Hernandez, G.A., and Gross, J.D. (2010). A split active site couples cap recognition by Dcp2 to activation. Nat Struct Mol Biol *17*, 1096-1101.

Fromm, S.A., Kamenz, J., Noldeke, E.R., Neu, A., Zocher, G., and Sprangers, R. (2014). In vitro reconstitution of a cellular phase-transition process that involves the mRNA decapping machinery. Angew Chem Int Ed Engl *53*, 7354-7359.

Georgiev, A., Sjostrom, M., and Wieslander, A. (2007). Binding specificities of the GYF domains from two Saccharomyces cerevisiae paralogs. Protein Eng Des Sel *20*, 443-452.

Gietz, R.D., and Schiestl, R.H. (2007). High-efficiency yeast transformation using the LiAc/SS carrier DNA/PEG method. Nat Protoc *2*, 31-34.

Harigaya, Y., Jones, B.N., Muhlrad, D., Gross, J.D., and Parker, R. (2010). Identification and analysis of the interaction between Edc3 and Dcp2 in Saccharomyces cerevisiae. Mol Cell Biol *30*, 1446-1456.

He, F., Brown, A. H., & Jacobson, A. (1997). Upf1p, Nmd2p, and Upf3p are interacting components of the yeast nonsense-mediated mRNA decay pathway. Mol Cell Biol *17*, 1580–1594.

Ho, B., Baryshnikova, A., and Brown, G.W. (2018). Unification of Protein Abundance Datasets Yields a Quantitative Saccharomyces cerevisiae Proteome. Cell Syst *6*, 192-205 e193.

Hubstenberger, A., Courel, M., Benard, M., Souquere, S., Ernoult-Lange, M., Chouaib, R., Yi, Z., Morlot, J.B., Munier, A., Fradet, M.*, et al.* (2017). P body Purification Reveals the Condensation of Repressed mRNA Regulons. Mol Cell *68*, 144-157 e145.

Ingelfinger, D., Arndt-Jovin, D.J., Lührmann, R., Achsel, T. (2002). The human LSm1-7 proteins colocalize with the mRNA-degrading enzymes Dcp1/2 and Xrn1 in distinct cytoplasmic foci. RNA *8*, 1489-1501.

Irie, K., Tadauchi, T., Takizawa, P. A., Vale, R. D., Matsumoto, K., and Herskowitz, I. (2002). The Khd1 protein, which has three KH RNA-binding motifs, is required for proper localization of *ASH1* mRNA in yeast. EMBO J *21*, 1158–1167.

Jain, S., Wheeler, J.R., Walters, R.W., Agrawal, A., Barsic, A., and Parker, R. (2016). ATPase-Modulated Stress Granules Contain a Diverse Proteome and Substructure. Cell *164*, 487-498.

Khong, A., Matheny, T., Jain, S., Mitchell, S.F., Wheeler, J.R., and Parker, R. (2017). The Stress Granule Transcriptome Reveals Principles of mRNA Accumulation in Stress Granules. Mol Cell *68*, 808-820 e805.

Knop, M., Siegers, K., Pereira, G., Zachariae, W., Winsor, B., Nasmyth, K., and Schiebel, E. (1999). Epitope tagging of yeast genes using a PCR-based strategy: more tags and improved practical routines. Yeast *15*, 963–972.

Klingauf, M., Sranek, D., and Neugebauer K.M. (2006). Enhancement of U4/U6 Small Nuclear Ribonucleoprotein Particle Association in Cajal Bodies Predicted by Mathematical Modeling. Mol Biol Cell *17*, 4972-81.

Krogan, N.J., Cagney, G., Yu, H., Zhong, G., Guo, X., Ignatchenko, A., Li, J., Pu, S., Datta, N., Tikuisis, A.P.*, et al.* (2006). Global landscape of protein complexes in the yeast Saccharomyces cerevisiae. Nature *440*, 637-643.

Kshirsagar, M., and Parker, R. (2004). Identification of Edc3p as an enhance of mRNA decapping in Saccharomyces verevisiae. Genetics *166*, 729-739.

Kurischko, C., Kim, H.K., Kuravi, V.K., Pratzka, J., and Luca, F.C. (2011). The yeast Cbk1 kinase regulates mRNA localization via the mRNA-binding protein Ssd1. J Cell Biol *192*, 583-598.

Lallemand-Breitenbach, V., and de The, H. (2010). PML nuclear bodies. Cold Spring Harb Perspect Biol *2*, a000661.

Larson, A.G., Elnatan, D., Keenen, M.M., Trnka, M.J., Johnston, J.B., Burlingame, A.L., Agard, D.A., Redding, S., and Narlikar, G.J. (2017). Liquid droplet formation by HP1alpha suggests a role for phase separation in heterochromatin. Nature *547*, 236-240.

Leung, A.K., Calabrese, J.M., Sharp, P.A. (2006) Quantitative analysis of Argonaute protein reveals microRNA-dependent localization to stress granules. Pro. Natl. Acad. Sci. USA *103*, 18125-18130.

Li, H., Leo, C., Zhu, J., Wu, X., O'Neil, J., Park, E., Chen, J. D. (2000). Sequestration and Inhibition of Daxx-Mediated Transcriptional Repression by PML. Mol Cell Biol *20*, 1784-1796.

Li, K., Zhao, K., Ossareh-Nazari, B., Da, G., Dargemont, C., and Marmorstein, R. (2005). Structural basis for interaction between the Ubp3 deubiquitinating enzyme and its Bre5 cofactor. J Biol Chem *280*, 29176-29185.

Li, P., Banjade, S., Cheng, H.C., Kim, S., Chen, B., Guo, L., Llaguno, M., Hollingsworth, J.V., King, D.S., Banani, S.F.*, et al.* (2012). Phase transitions in the assembly of multivalent signalling proteins. Nature *483*, 336-340.

Lin, Y., Protter, D.S., Rosen, M.K., and Parker, R. (2015). Formation and Maturation of Phase-Separated Liquid Droplets by RNA-Binding Proteins. Mol Cell *60*, 208-219.

Lotan, R., Bar-On, V.G., Harel-Sharvit, L., Duek, L., Melamed, D., and Choder, M. (2005). The RNA polymerase II subunit Rpb4p mediates decay of a specific class of mRNAs. Genes Dev *19*, 3004–3016.

Lotan, R., Goler-Baron, V., Duek, L., Haimovich, G., and Choder, M. (2007). The Rpb7p subunit of yeast RNA polymerase II plays roles in the two major cytoplasmic mRNA decay mechanisms. J Cell Biol *178*, 1133-1143.

Malys, N., and McCarthy, J.E. (2006). Dcs2, a novel stress-induced modulator of m7GpppX pyrophosphatase activity that locates to P bodies. J Mol Biol *363*, 370-382.

Markmiller, S., Soltanieh, S., Server, K.L., Mak, R., Jin, W., Fang, M.Y., Luo, E.C., Krach, F., Yang, D., Sen, A.*, et al.* (2018). Context-Dependent and Disease-Specific Diversity in Protein Interactions within Stress Granules. Cell *172*, 590-604 e513.

Mitchell, S.F., Jain, S., She, M., and Parker, R. (2013). Global analysis of yeast mRNPs. Nat Struct Mol Biol *20*, 127-133.

Mugler, C.F., Hondele, M., Heinrich, S., Sachdev, R., Vallotton, P., Koek, A.Y., Chan, L.Y., and Weis, K. (2016). ATPase activity of the DEAD-box protein Dhh1 controls processing body formation. Elife *5*.

Neef, D.W., and Thiele, D.J. (2009). Enhancer of decapping proteins 1 and 2 are important for translation during heat stress in *Saccharomyces cerevisiae*. Mol Microbiol, *73*, 1032–1042.

Nissan, T., Rajyaguru, P., She, M., Song, H., and Parker, R. (2010). Decapping activators in Saccharomyces cerevisiae act by multiple mechanisms. Mol Cell *39*, 773-783.

Pedro-Segura, E., Vergara, S.V., Rodríguez-Navarro, S., Parker, R., Thiele, D. J., and Puig, S. (2008). The Cth2 ARE-binding Protein Recruits the Dhh1 Helicase to Promote the Decay of Succinate Dehydrogenase *SDH4* mRNA in Response to Iron Deficiency. J Biol Chem 283, 28527–28535.

Pilkington, G.R., and Parker, R. (2008). Pat1 contains distinct functional domains that promote P body assembly and activation of decapping. Mol Cell Biol *28*, 1298-1312.

Protter, D.S.W., Rao, B.S., Van Treeck, B., Lin, Y., Mizoue, L., Rosen, M.K., and Parker, R. (2018). Intrinsically Disordered Regions Can Contribute Promiscuous Interactions to RNP Granule Assembly. Cell Rep *22*, 1401-1412.

Rajyaguru, P., She, M., and Parker, R. (2012). Scd6 targets eIF4G to repress translation: RGG motif proteins as a class of eIF4G-binding proteins. Mol Cell *45*, 244-254.

Rao, B.S., and Parker, R. (2017). Numerous interactions act redundantly to assemble a tunable size of P bodies in Saccharomyces cerevisiae. Proc Natl Acad Sci U S A *114*, E9569-E9578.

Riback, J.A., Katanski, C.D., Kear-Scott, J.L., Pilipenko, E.V., Rojek, A.E., Sosnick, T.R., and Drummond, D.A. (2017). Stress-Triggered Phase Separation Is an Adaptive, Evolutionarily Tuned Response. Cell *168*, 1028-1040 e1019.

Saha, S., Weber, C.A., Nousch, M., Adame-Arana, O., Hoege, C., Hein, M.Y., Osborne-Nishimura, E., Mahamid, J., Jahnel, M., Jawerth, L.*, et al.* (2016). Polar Positioning of Phase-Separated Liquid Compartments in Cells Regulated by an mRNA Competition Mechanism. Cell *166*, 1572-1584 e1516.

Schütz, S., Noldeke, E.R., and Sprangers, R. (2017). A synergistic network of interactions promotes the formation of in vitro processing bodies and protects mRNA against decapping. Nucleic Acids Res *45*, 6911-6922.

Schwartz, D., Decker, C. J., and Parker, R. (2003). The enhancer of decapping proteins, Edc1p and Edc2p, bind RNA and stimulate the activity of the decapping enzyme. RNA *9*, 239–251.

Sharif, H., and Conti, E. (2013). Architecture of the Lsm1-7-Pat1 complex: a conserved assembly in eukaryotic mRNA turnover. Cell Rep *5*, 283-291.

Sheth, U., Parker, R. (2003). Decapping and Decay of Messenger RNA Occur in Cytoplasmic Processing Bodies. Science *300*, 805-808.

Sheth, U., and Parker, R. (2006). Targeting of aberrant mRNAs to cytoplasmic processing bodies. Cell *125*, 1095-1109.

Shin, Y., and Brangwynne, C.P. (2017). Liquid phase condensation in cell physiology and disease. Science *357*.

Simpson, C.E., Lui, J., Kershaw, C.J., Sims, P.F., and Ashe, M.P. (2014). mRNA localization to P bodies in yeast is bi-phasic with many mRNAs captured in a late Bfr1p-dependent wave. J Cell Sci *127*, 1254-1262.

Smith, J., Calidas, D., Schmidt, H., Lu, T., Rasoloson, D., and Seydoux, G. (2016). Spatial patterning of P granules by RNA-induced phase separation of the intrinsically-disordered protein MEG-3. Elife *5*.

Strom, A.R., Emelyanov, A.V., Mir, M., Fyodorov, D.V., Darzacq, X., and Karpen, G.H. (2017). Phase separation drives heterochromatin domain formation. Nature *547*, 241-245.

Su, X., Ditlev, J.A., Hui,E., Xing, W., Julia Okrut, J., King, D.S., Taunton, J., Rosen, M.K., Vale, R.D. (2016). Phase separation of signaling molecules promotes T cell receptor signal transduction. Science *352*, 595-599.

Sweet, T.J., Boyer, B., Hu, W., Baker, K.E., and Coller, J. (2007). Microtubule disruption stimulates P body formation. RNA *13*, 493-502.

Swisher, K.D., and Parker, R. (2011). Interactions between Upf1 and the decapping factors Edc3 and Pat1 in Saccharomyces cerevisiae. PLoS One *6*, e26547.

Teixeira, D., Sheth, U., Valencia-Sanchez, M.A., Brengues, M., and Parker, R. (2005). Processing bodies require RNA for assembly and contain nontranslating mRNAs. RNA *11*, 371-382.

Teixeira, D., Parker, R. (2007). Analysis of P body Assembly in Saccharomyces cerevisiae. Mol Biol Cell *18*, 2274-2287.

Uchida, M., Sun, Y., McDermott, G., Knoechel, C., Le Gros, M.A., Parkinson, D., Drubin, D.G., and Larabell, C.A. (2011). Quantitative analysis of yeast internal architecture using soft X-ray tomography. Yeast *28*, 227-236.

Uesono, Y., Toh-e, A., and Kikuchi, Y. (1997). Ssd1p of Saccharomyces cerevisiae Associates with RNA. J Biol Chem *272*, 16103-16109.

van Dijk, E., Cougot, N., Meyer, S., Babajko, S., Wahle, E., Séraphin, B. (2002). Human Dcp2: a catalytically active mRNA decapping enzyme located in specific cytoplasmic structures. EMBO J *21*, 6915-6924.

Wang, J.T., Smith, J., Chen, B.C., Schmidt, H., Rasoloson, D., Paix, A., Lambrus, B.G., Calidas, D., Betzig, E., and Seydoux, G. (2014). Regulation of RNA granule dynamics

by phosphorylation of serine-rich, intrinsically disordered proteins in C. elegans. Elife *3*, e04591.

Wei, M.T., Elbaum-Garfinkle, S., Holehouse, A.S., Chen, C.C., Feric, M., Arnold, C.B., Priestley, R.D., Pappu, R.V., and Brangwynne, C.P. (2017). Phase behaviour of disordered proteins underlying low density and high permeability of liquid organelles. Nat Chem *9*, 1118-1125.

Weidtkamp-Peters, S., Lenser, T., Negorev, D., Gerstner, N., Hofmann, T.G., Schwanitz, G., Hoischen, C., Maul, G., Dittrich, P., and Hemmerich, P. (2008). Dynamics of component exchange at PML nuclear bodies. J Cell Sci *121*, 2731-2743.

Wheeler, J.R., Jain, S., Khong, A., and Parker, R. (2017). Isolation of yeast and mammalian stress granule cores. Methods *126*, 12-17.

Woodruff, J.B., Ferreira Gomes, B., Widlund, P.O., Mahamid, J., Honigmann, A., and Hyman, A.A. (2017). The Centrosome Is a Selective Condensate that Nucleates Microtubules by Concentrating Tubulin. Cell *169*, 1066-1077 e1010.

Yamaguchi, M., Namiki, Y., Okada, H., Mori, Y., Furukawa, H., Wang, J., Ohkusu, M., and Kawamoto, S. (2011). Structome of Saccharomyces cerevisiae determined by freeze-substitution and serial ultrathin-sectioning electron microscopy. J Electron Microsc (Tokyo) *60*, 321-335.

Youn, J.Y., Dunham, W.H., Hong, S.J., Knight, J.D.R., Bashkurov, M., Chen, G.I., Bagci, H., Rathod, B., MacLeod, G., Eng, S.W.M.*, et al.* (2018). High-Density Proximity Mapping Reveals the Subcellular Organization of mRNA-Associated Granules and Bodies. Mol Cell *69*, 517-532 e511.

Figure 1

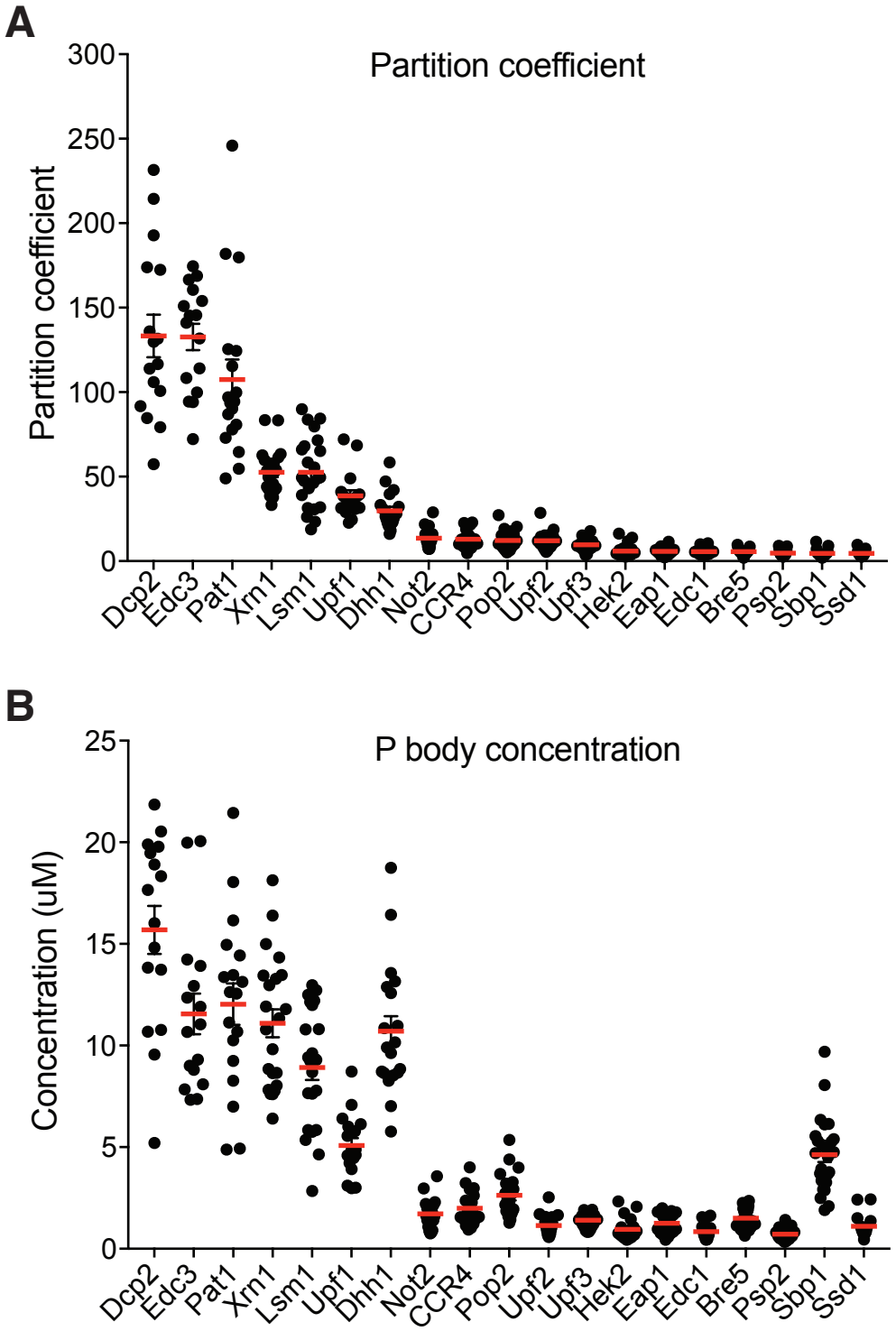
A
Partition coefficient
Partition coefficient
300
250
200
150
100
50
0
Dcp2
Edc3
Pat1
Xrn1
Lsm1
Upf1
Dhh1
Not2
CCR4
Pop2
Upf2
Upf3
Hek2
Eap1
Edc1
Bre5
Psp2
Sbp1
Ssd1
B
P body concentration
Concentration (uM)
25
20
15
10
5
0
Dcp2
Edc3
Pat1
Xrn1
Lsm1
Upf1
Dhh1
Not2
CCR4
Pop2
Upf2
Upf3
Hek2
Eap1
Edc1
Bre5
Psp2
Sbp1
Ssd1

Figure 2

A

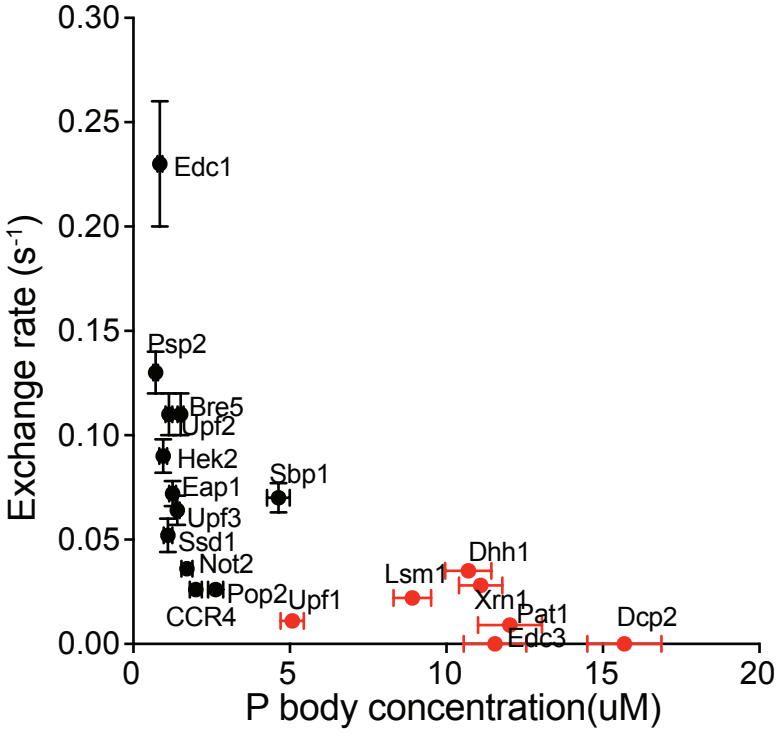
Exchange rate (s-1)
0.30
0.25
0.20
0.15
0.10
0.05
0.00
Edc1
Psp2
Bre5
Upf2
Hek2
Eap1
Sbp1
Upf3
Ssd1
Not2
Pop2
CCR4
Upf1
Lsm1
Dhh1
Xrn1
Pat1
Edc3
Dcp2
0
5
10
15
20
P body concentration(uM)

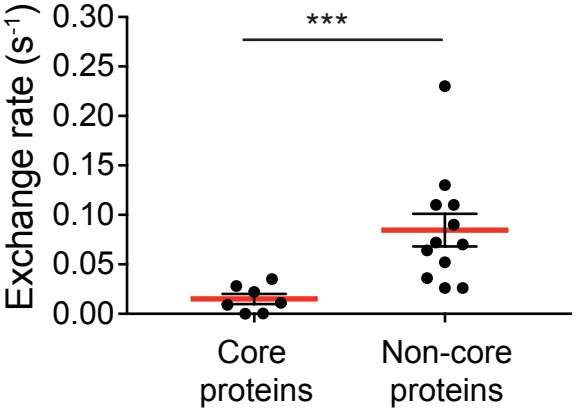
Exchange rate (s-1)
0.30
0.25
0.20
0.15
0.10
0.05
0.00
***
Core proteins
Non-core proteins

B

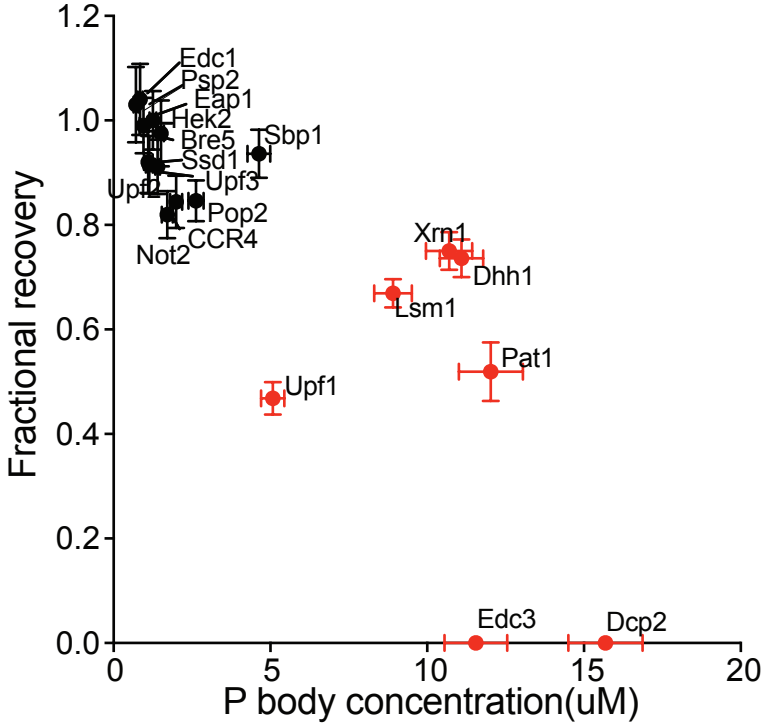
Fractional recovery
1.2
1.0
0.8
0.6
0.4
0.2
0.0
Edc1
Psp2
Eap1
Hek2
Bre5
Sbp1
Ssd1
Upf2
Upf3
Pop2
CCR4
Not2
Xrn1
Dhh1
Lsm1
Pat1
Upf1
Edc3
Dcp2
0
5
10
15
20
P body concentration(uM)

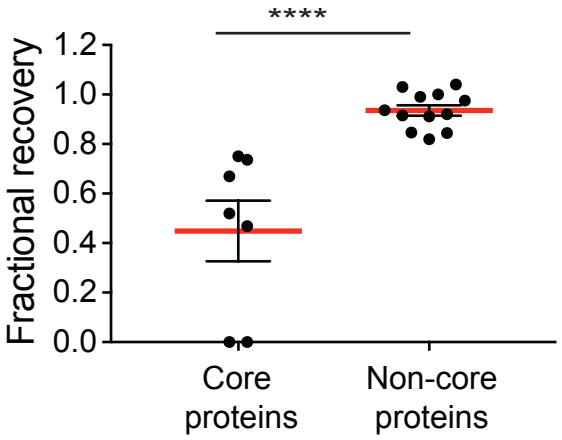
Fractional recovery
1.2
1.0
0.8
0.6
0.4
0.2
0.0
****
Core proteins
Non-core proteins

Figure 3

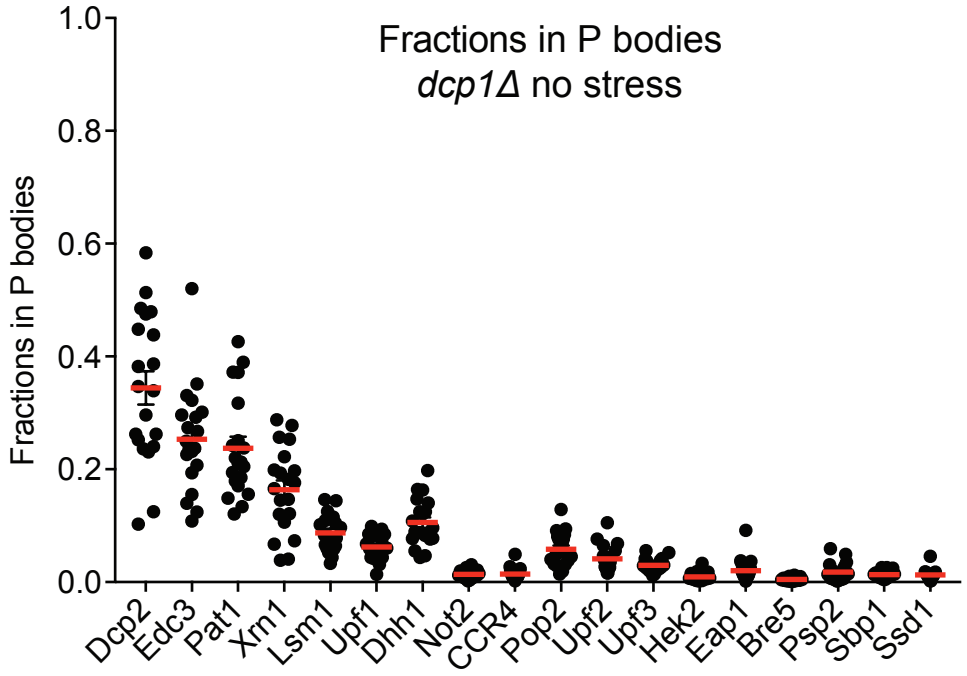
Fractions in P bodies
dcp1Δ no stress
Fractions in P bodies
1.0
0.8
0.6
0.4
0.2
0.0
Dcp2
Edc3
Pat1
Xrn1
Lsm1
Upf1
Dhh1
Not2
CCR4
Pop2
Upf2
Upf3
Hek2
Eap1
Bre5
Psp2
Sbp1
Ssd1

Figure 4

A

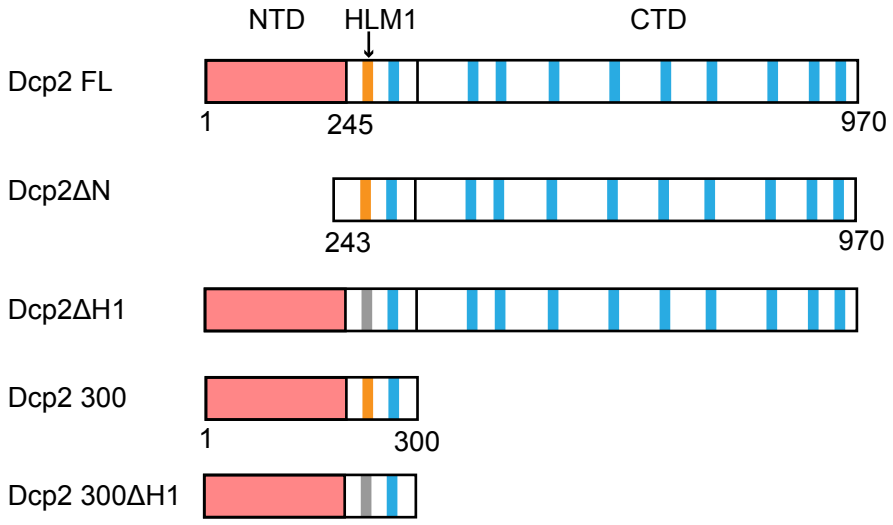

B

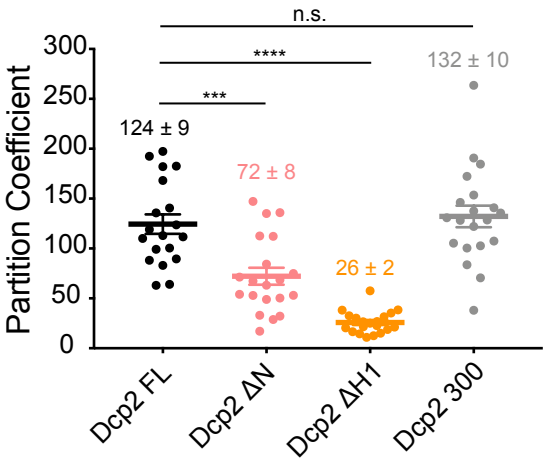

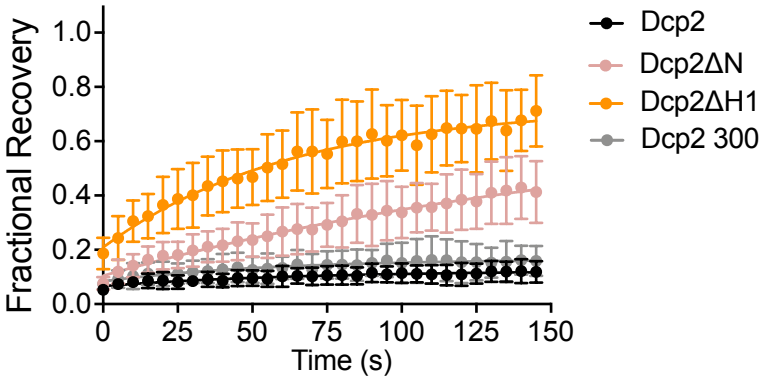

C

Dcp2 ΔH1 vs Dcp2 300ΔH1

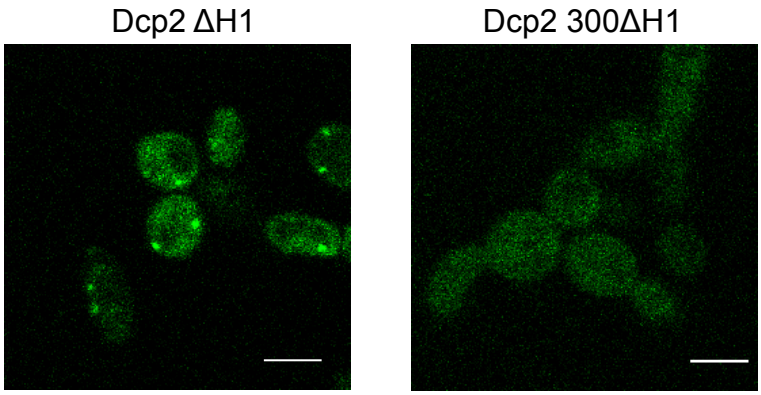

Figure 5

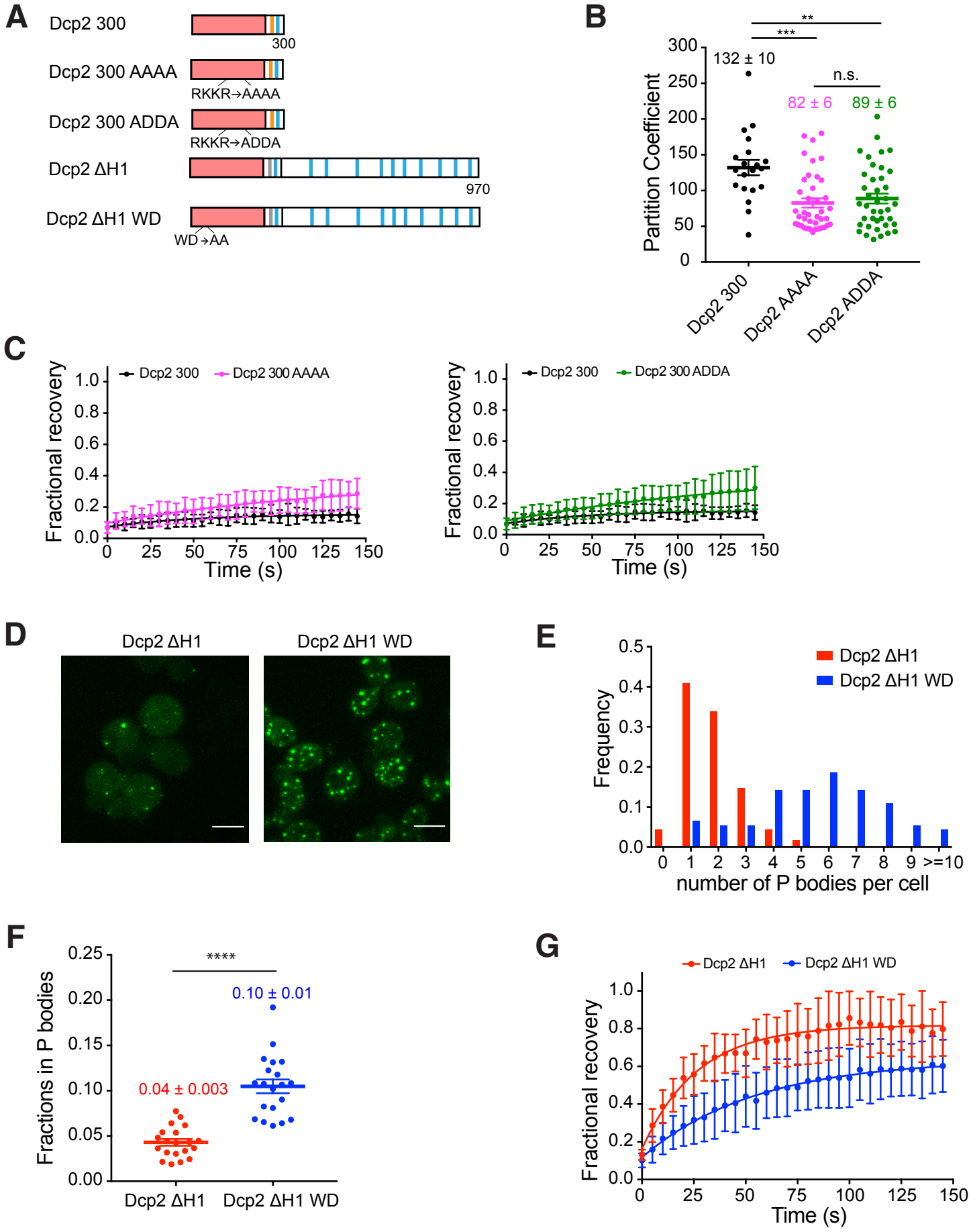
A
Dcp2 300
300
Dcp2 300 AAAA
RKKR→AAAA
Dcp2 300 ADDA
RKKR→ADDA
Dcp2 ΔH1
970
Dcp2 ΔH1 WD
WD→AA
B
Partition Coefficient
132 ± 10
82 ± 6
89 ± 6
**
***
n.s.
Dcp2 300
Dcp2 AAAA
Dcp2 ADDA
C
Fractional recovery
Time (s)
Dcp2 300
Dcp2 300 AAAA
Dcp2 300 ADDA
D
Dcp2 ΔH1
Dcp2 ΔH1 WD
E
Frequency
number of P bodies per cell
Dcp2 ΔH1
Dcp2 ΔH1 WD
F
Fractions in P bodies
****
0.04 ± 0.003
0.10 ± 0.01
Dcp2 ΔH1
Dcp2 ΔH1 WD
G
Fractional recovery
Time (s)
Dcp2 ΔH1
Dcp2 ΔH1 WD

Figure 6

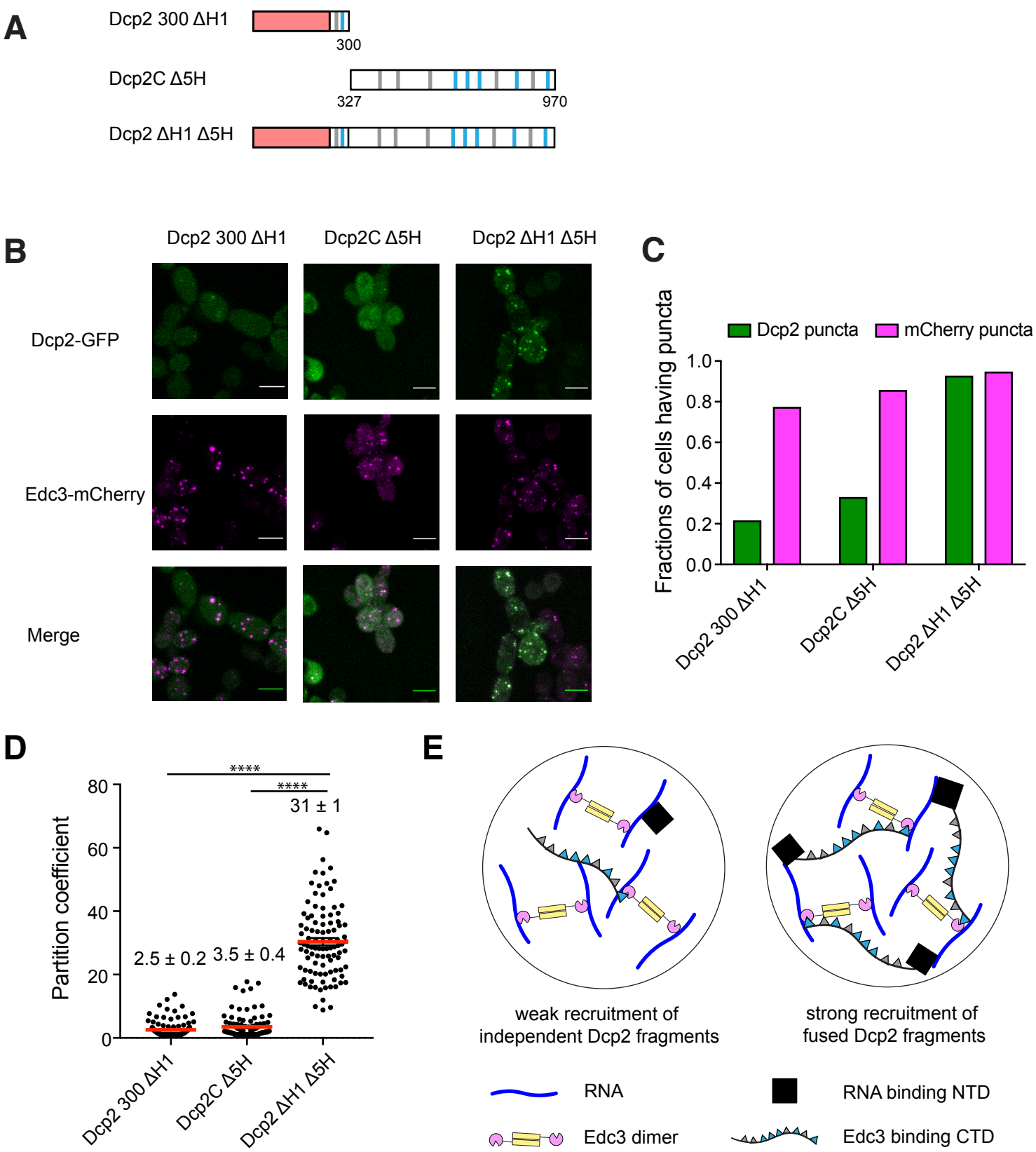
A
Dcp2 300 ΔH1
300
Dcp2C Δ5H
327
970
Dcp2 ΔH1 Δ5H
B
Dcp2 300 ΔH1
Dcp2C Δ5H
Dcp2 ΔH1 Δ5H
Dcp2-GFP
Edc3-mCherry
Merge
C
Dcp2 puncta
mCherry puncta
Fractions of cells having puncta
1.0
0.8
0.6
0.4
0.2
0.0
Dcp2 300 ΔH1
Dcp2C Δ5H
Dcp2 ΔH1 Δ5H
D
Partition coefficient
80
60
40
20
0
****
****
31 ± 1
2.5 ± 0.2
3.5 ± 0.4
Dcp2 300 ΔH1
Dcp2C Δ5H
Dcp2 ΔH1 Δ5H
E
weak recruitment of
independent Dcp2 fragments
strong recruitment of
fused Dcp2 fragments
RNA
RNA binding NTD
Edc3 dimer
Edc3 binding CTD

Figure 7

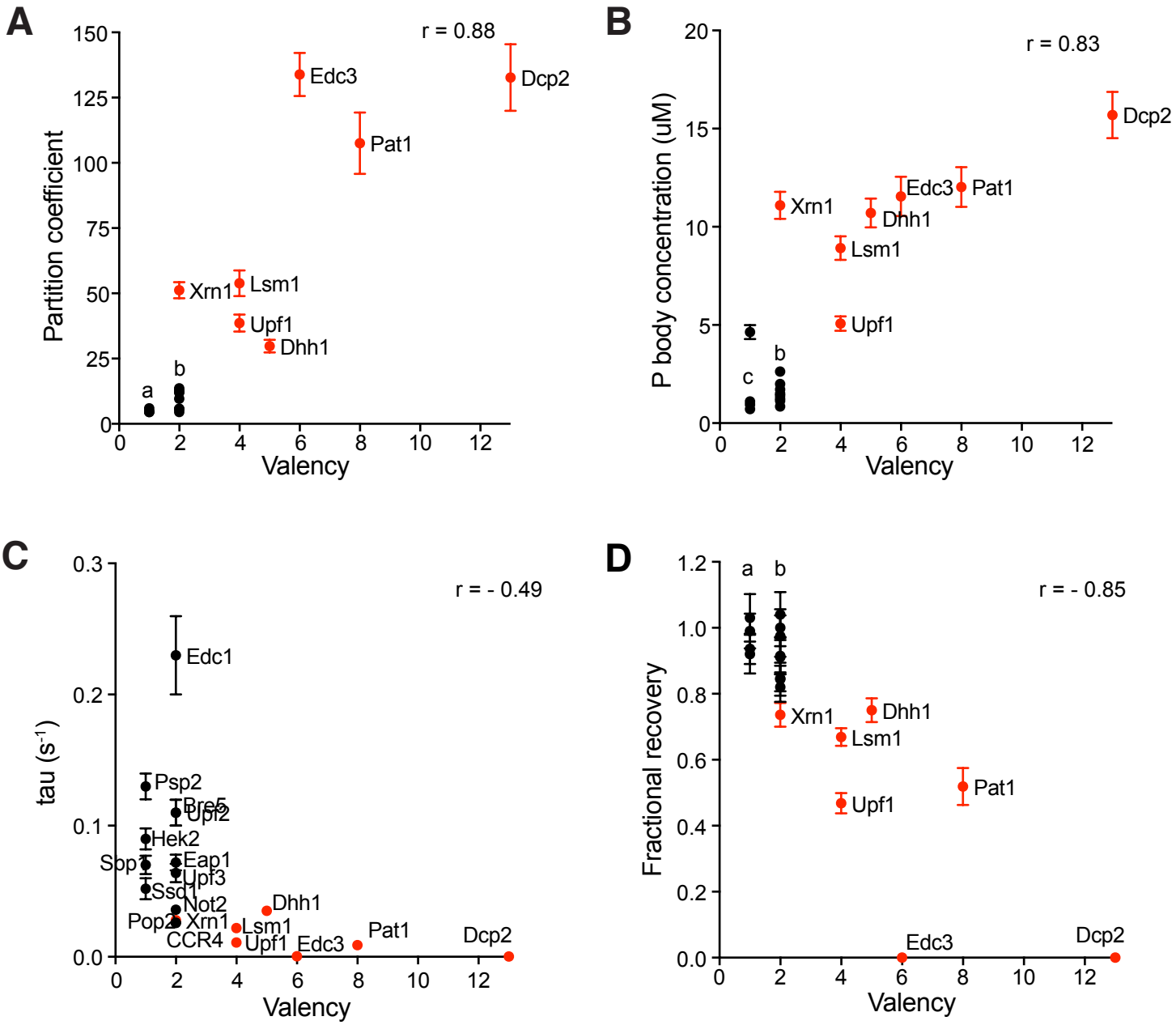

a. Psp2, Hek2, Sbp1, Ssd1
b. Edc2, Eap1, Bre5, Upf2, Upf3, Pop2, CCR4, Not2
c. Psp2, Hek2, Ssd1

Figure S1 related to Figure 1

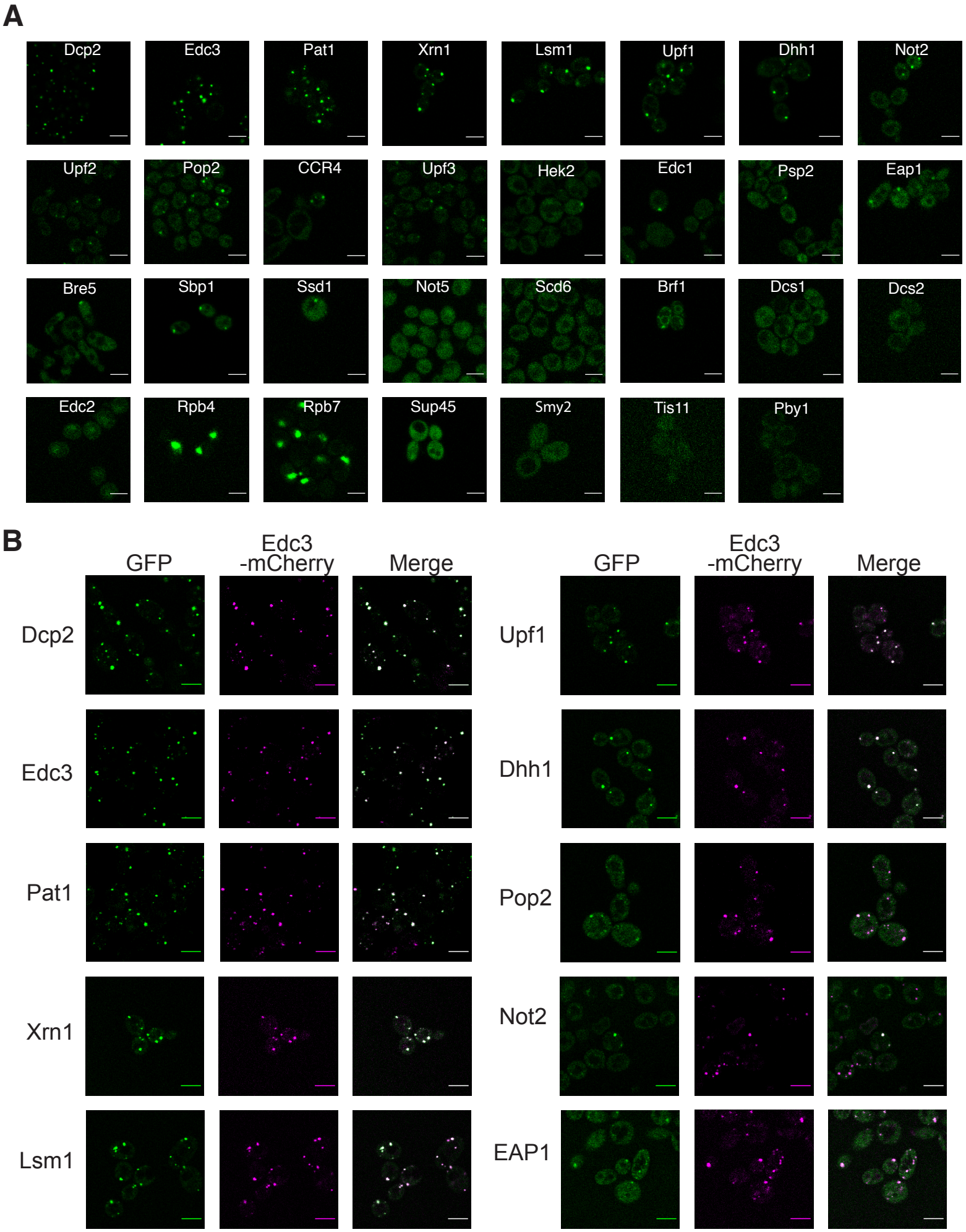

Figure S2 related to Figure 1, Figure 2

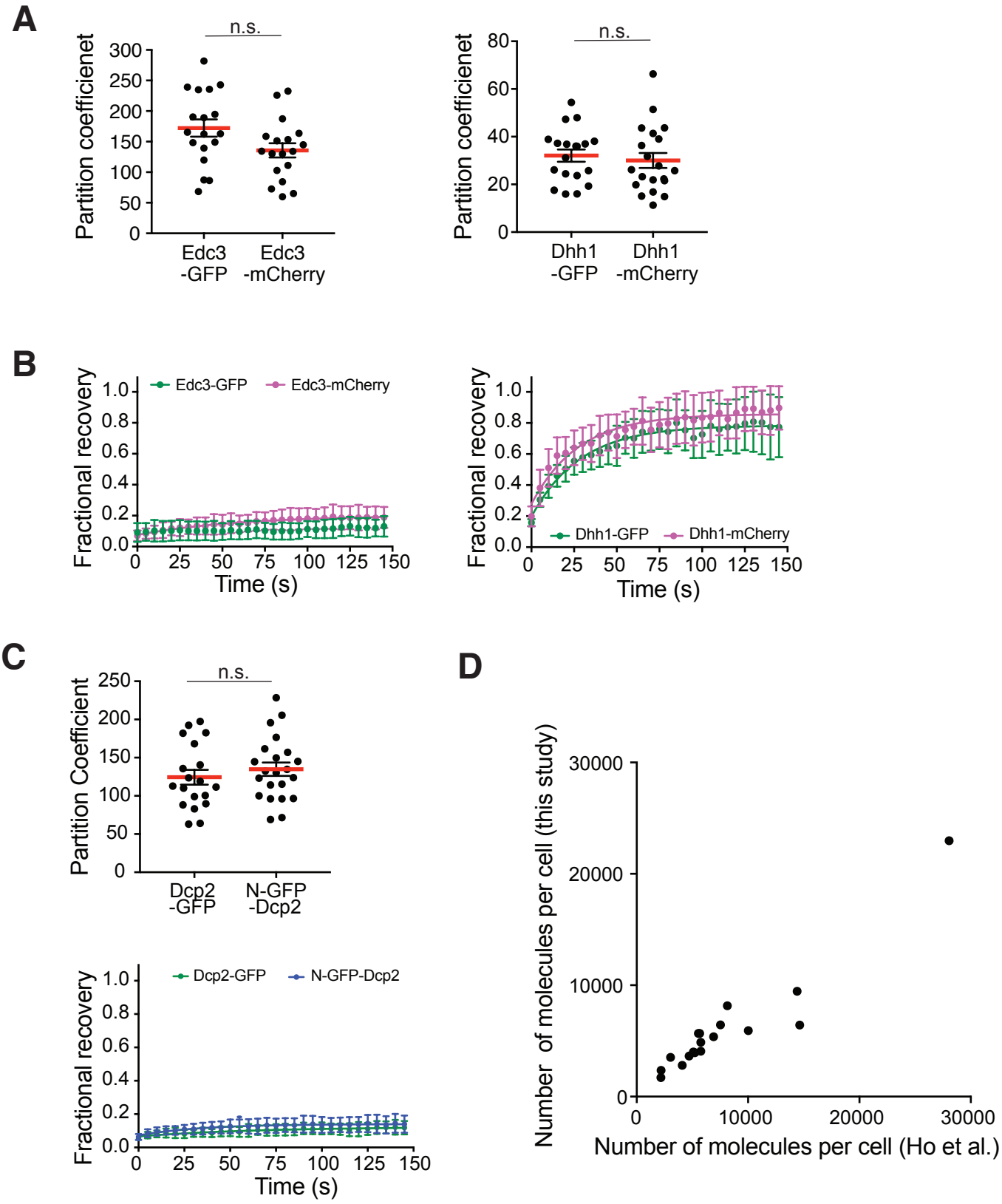

Figure S3 related to Figure 2

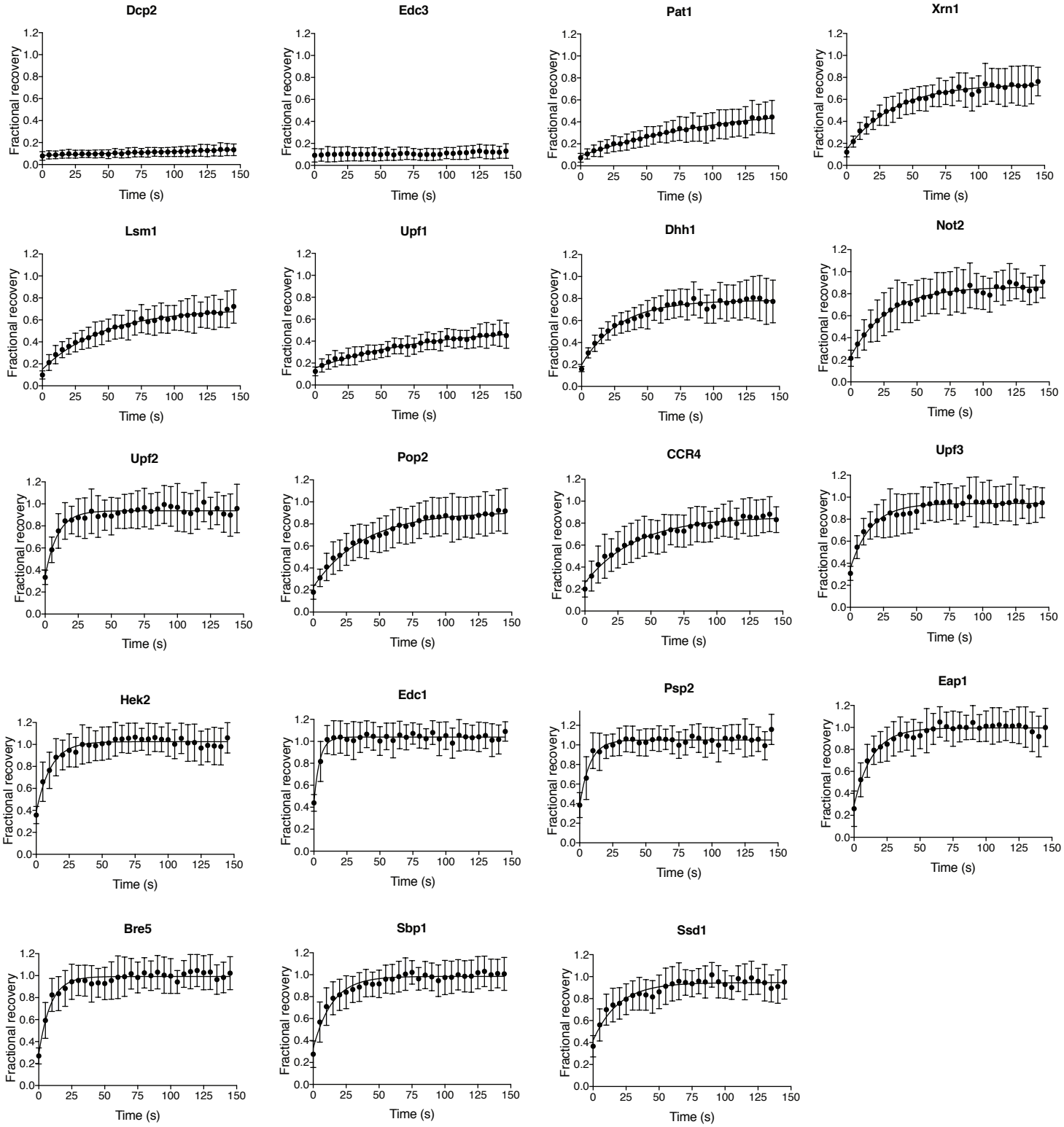

Figure S4 related to Figure 2

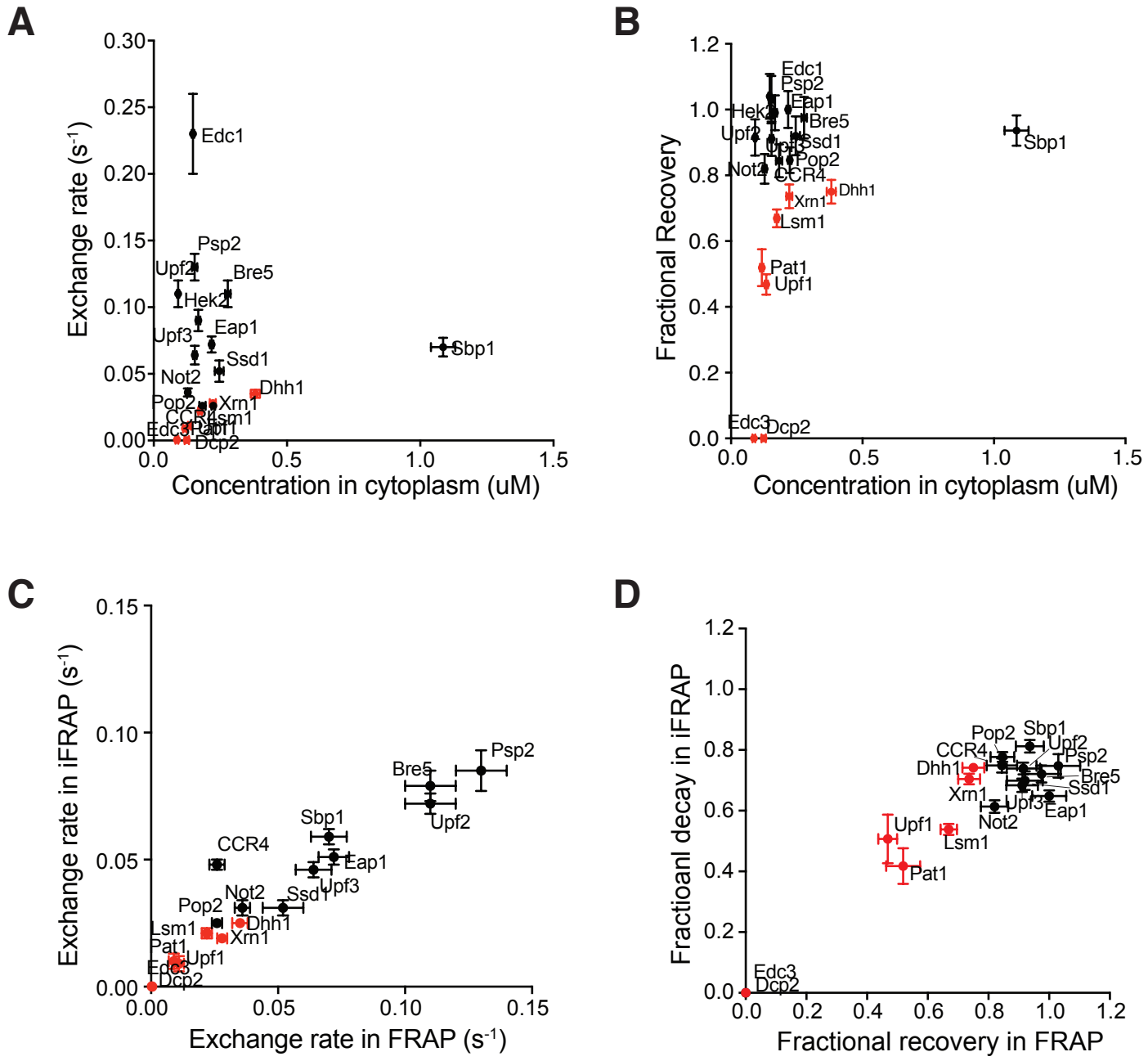

Figure S5 related to Figure 1 and Figure 2

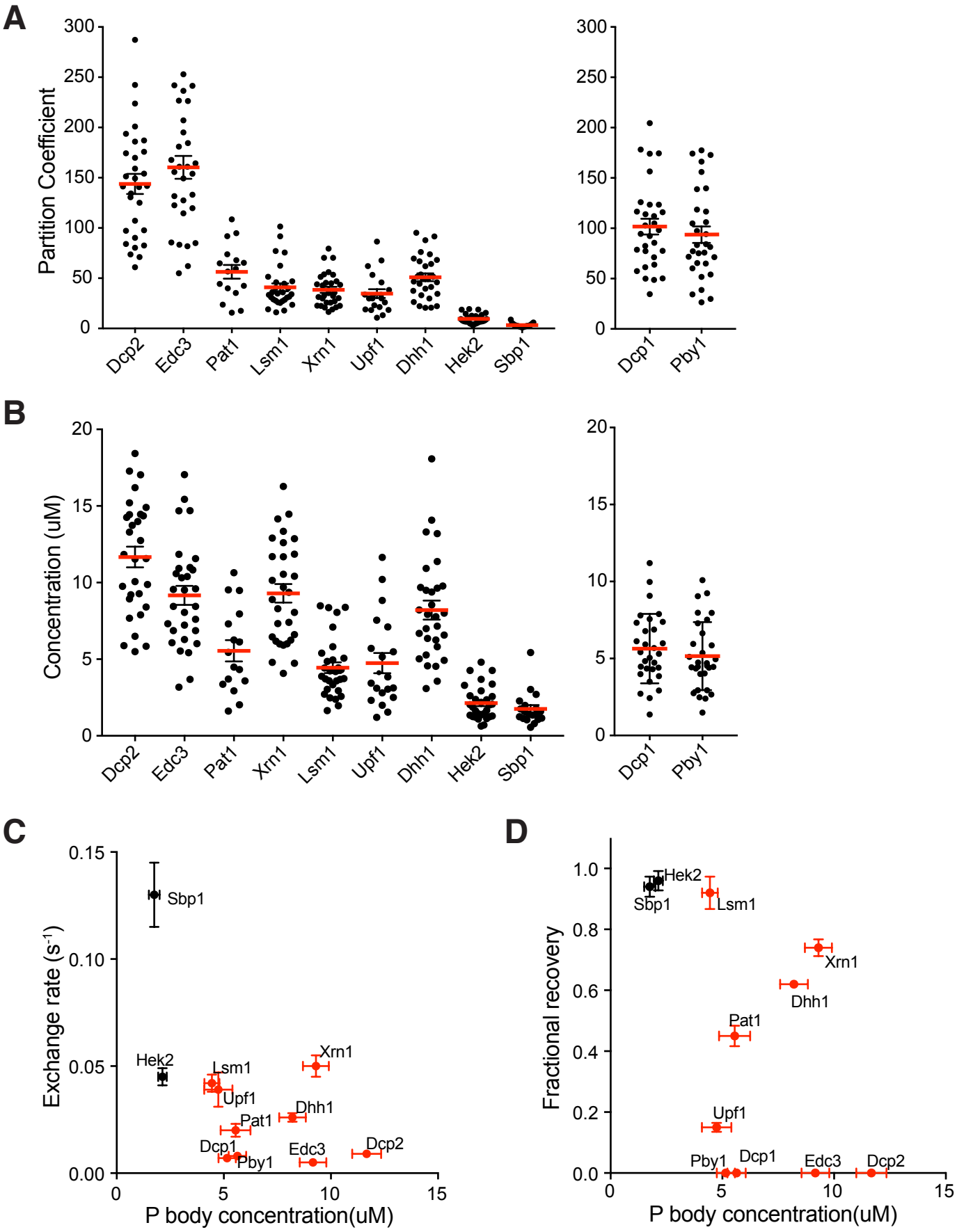

Figure S6 related to Figure 3

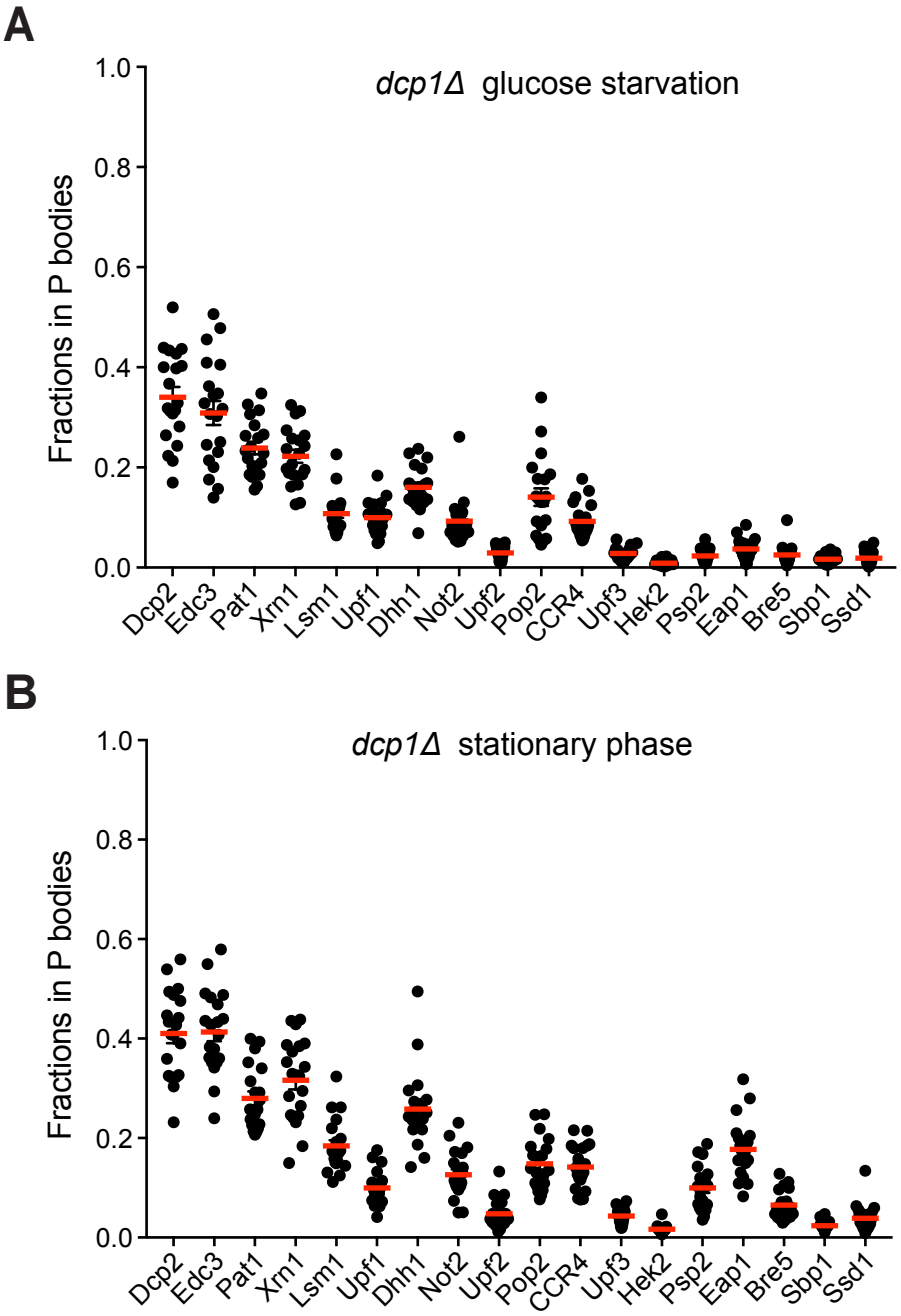

Figure S7 related to Figure 4, Figure 5, and Figure 6

A

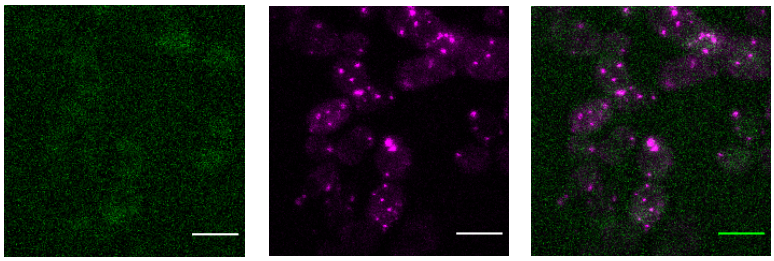

B

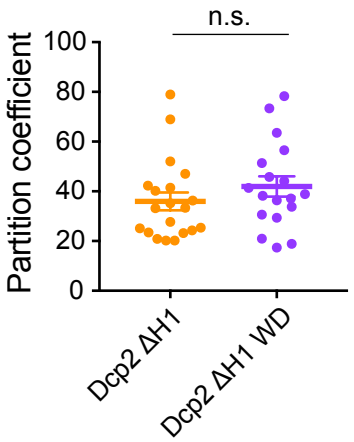

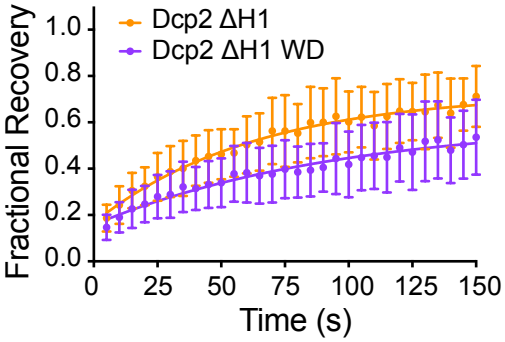

C

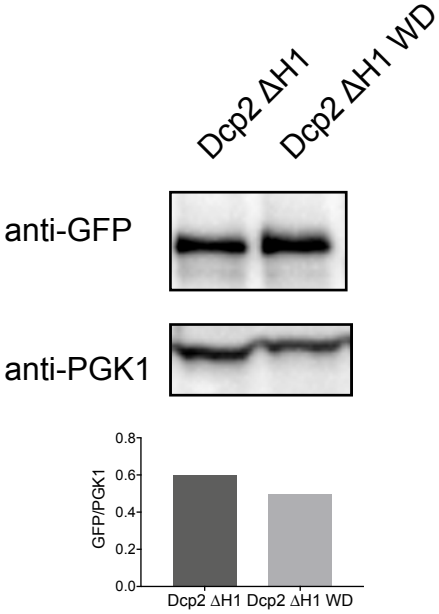

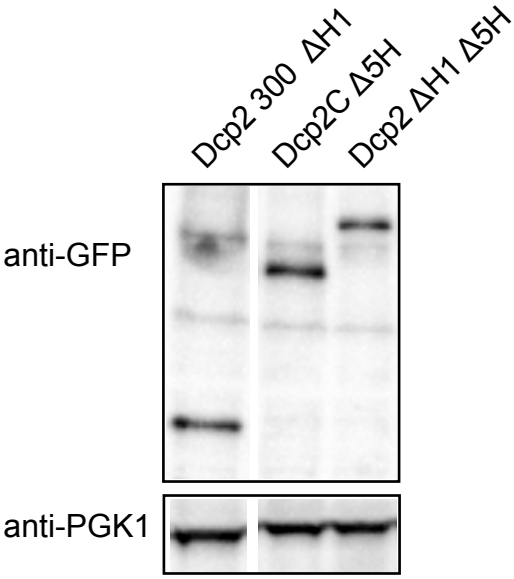

Table S1. Dynamics and partitioning of P body proteins*

Proteins	Partition Coefficient	P body concentrations (uM)	Cytoplasm concentrations (uM)	Exchange rate (s^{-1})**	Fractional recovery
Dcp2	133 ± 13	15 ± 1	0.12 ± 0.01	~ 0.0003***	0
Edc3	133 ± 8	12 ± 1	0.09 ± 0.01	~ 0.0005***	0
Pat1	107 ± 12	12 ± 1	0.12 ± 0.01	0.009 ± 0.002	0.52 ± 0.06
Xrn1	53 ± 3	11 ± 1	0.22 ± 0.01	0.028 ± 0.002	0.74 ± 0.04
Lsm1	52 ± 4	8.9 ± 0.6	0.17 ± 0.01	0.022 ± 0.002	0.67 ± 0.03
Upf1	39 ± 3	5.1 ± 0.4	0.13 ± 0.01	0.011 ± 0.002	0.47 ± 0.03
Dhh1	30 ± 2	10 ± 1	0.38 ± 0.02	0.035 ± 0.003	0.75 ± 0.04
Not2	12 ± 1	1.6 ± 0.2	0.13 ± 0.01	0.036 ± 0.003	0.82 ± 0.05
Upf2	12 ± 1	1.0 ± 0.1	0.09 ± 0.01	0.11 ± 0.01	0.92 ± 0.06
Pop2	11 ± 1	2.4 ± 0.2	0.22 ± 0.01	0.026 ± 0.002	0.85 ± 0.04
CCR4	10 ± 1	1.8 ± 0.2	0.18 ± 0.01	0.026 ± 0.003	0.84 ± 0.05
Upf3	8.6 ± 0.7	1.3 ± 0.1	0.15 ± 0.01	0.064 ± 0.007	0.91 ± 0.05
Hek2	5.9 ± 0.8	1.0 ± 0.1	0.16 ± 0.01	0.091 ± 0.008	0.99 ± 0.05
Edc1	5.7 ± 0.5	0.8 ± 0.1	0.15 ± 0.01	0.23 ± 0.03	1.00 ± 0.07
Psp2	4.8 ± 0.5	0.7 ± 0.1	0.15 ± 0.01	0.13 ± 0.01	1.00 ± 0.07
Eap1	4.8 ± 0.5	1.0 ± 0.1	0.22 ± 0.01	0.072 ± 0.006	1.00 ± 0.06
Bre5	4.6 ± 0.4	1.2 ± 0.1	0.28 ± 0.01	0.11 ± 0.01	0.97 ± 0.06
Sbp1	4.5 ± 0.4	4.6 ± 0.4	1.1 ± 0.05	0.069 ± 0.007	0.94 ± 0.05
Ssd1	4.5 ± 0.4	1.1 ± 0.1	0.25 ± 0.02	0.052 ± 0.008	0.92 ± 0.06

* Mean ± SEM for partitioning coefficient, P body concentrations, Cytoplasm concentrations, Exchange rate and Fractional recovery.
** Exchange rate is exponential rate constant of exchange (k).
*** FRAP curves of Dcp2 and Edc3 are almost flat that the software can only fit ambiguous values.

Table S2. Yeast strains used in this study

Yeast Strains	note	genotype	P body localization	Explanation for lacking of P body localization in *dcp1*Δ strain	Reference
yRP3156	*dcp1*Δ *dcp2*Δ	*Mat a his4-539 leu2-3,112 lys2-201 trp1 ura3-52 dcp1::URA3(5FOA+) dcp2::TRP1 cup1::LEU2/PGK1pG/MFA2pG*			
yRP1346	*dcp2*Δ	*Mat a his4-539 leu2-3,112 lys2-201 trp1 ura3-52 dcp2::TRP1 cup1::LEU2/PGK1pG/MFA2pG*			
yRP1936	*dcp1*Δ Dcp2	*Mat a leu2-3,112 cup1::LEU2/PGK1pG/MFA2pG his4-539 trp1 ura3-52 DCP2-GFP(NEO) dcp1::URA3*	Y		Sheth *et al* 2003
yRP2254	*dcp1*Δ Edc3	*Mat a leu2-3,112 trp1 ura3-52 his4-539 lys2-201 cup1::LEU2/PGK1pG/MFA2pG dcp1::URA3 EDC3-GFP (NEO)*	Y		Kshirsagar *et al* 2004
yRP2237	*dcp1*Δ Pat1	*Mat a leu2-3,112 trp1 ura3-52 his4-539 cup1::LEU2/PGK1pG/MFA2pG dcp1::URA3 PAT1-GFP (NEO)*	Y		Sheth *et al* 2003
yRP2246	*dcp1*Δ Xrn1	*Mat a leu2-3,112 trp1 ura3-52 his4-539 cup1::LEU2/PGK1pG/MFA2pG dcp1::URA3 XRN1-GFP (NEO)*	Y		Sheth *et al* 2003
yRP2230	*dcp1*Δ Lsm1	*Mat a leu2-3,112 trp1 ura3-52 his4-539 cup1::LEU2/PGK1pG/MFA2pG dcp1::URA3 LSM1-GFP (NEO)*	Y		Sheth *et al* 2003
yRP1840	*dcp1*Δ Upf1	*Mat a leu2-3,112 trp1 ura3-52 his4-539 cup1::LEU2/PGK1pG/MFA2pG dcp1::URA3 UPF1-GFP (NEO)*	Y		Sheth *et al* 2006
yRP1736	*dcp1*Δ Dhh1	*Mat a leu2-3,112 trp1 ura3-52 his4-539 cup1::LEU2/PGK1pG/MFA2pG dcp1::URA3 DHH1-GFP (NEO)*	Y		Sheth *et al* 2003
yRP2269	*dcp1*Δ Pop2	*Mat a leu2-3,112 trp1 ura3-52 his4-539 cup1::LEU2/PGK1pG/MFA2pG dcp1::URA3 POP2-GFP (NEO)*	Y		Sheth *et al* 2003, Teixeira *et al* 2007
yRP1844	*dcp1*Δ Upf3	*Mat a leu2-3.112 ura3-52 cup1::LEU2/PGK1pG/MFA2pG, dcp1::URA3, UPF3-GFP (NEO)*	Y		Sheth *et al* 2006
yRP1916	*dcp1*Δ Not2	*Mat alpha leu2-3,112 cup1::LEU2/PGK1pG/MFA2pG trp1 his4-539 ura3-52 dcp1::URA3 NOT2-GFP(NEO)*	Y		Sheth *et al* 2003, Teixeira *et al* 2007
yRP1842	*dcp1*Δ Upf2	*Mat a leu2-3,112, ura3-52 cup1::LEU2/PGK1pG/MFA2pG, dcp1:: URA3, UPF2-GFP(NEO)*	Y		Sheth *et al* 2006
yRP2261	*dcp1*Δ CCR4	*Mat a leu2-3,112 trp1 ura3-52 his4-539 cup1::LEU2/PGK1pG/MFA2pG dcp1::URA3 CCR4-GFP (NEO)*	Y		Sheth *et al* 2003, Teixeira *et al* 2007
yRP3140	*dcp1*Δ Hek2	*Mat a leu2, ura3, his3, met15, dcp1::URA3 HEK2::GFP(HIS3MX6)*	Y		Mitchell *et al* 2013
yRP3137	*dcp1*Δ Sbp1	*Mat alpha leu2, ura3, his3, met15, dcp1::URA3 SBP1::GFP(HIS3MX6)*	Y		Mitchell et al 2013
yRP3154	*dcp1*Δ Edc1	*Mat a leu2, ura3, his3, met15, dcp1::URA3 EDC1::GFP(HIS3MX6)*	Y		Neef *et al* 2009
yRP3143	*dcp1*Δ Bre5	*Mat a leu2, ura3, his3, met15, dcp1::URA3 BRE5::GFP(HIS3MX6)*	Y		Mitchell *et al* 2013
yRP3136	*dcp1*Δ Psp2	*Mat a leu2, ura3, his3, met15, dcp1::URA3 PSP2::GFP(HIS3MX6)*	Y		Mitchell *et al* 2013
yRP3146	*dcp1*Δ Eap1	*Mat a leu2, ura3, his3, met15, dcp1::URA3 EAP1::GFP(HIS3MX6)*	Y		Mitchell *et al* 2013
yRP3149	*dcp1*Δ Ssd1	*Mat a leu2, ura3, his3, met15, dcp1::URA3 SSD1::GFP(HIS3MX6)*	Y		Kurischko *et al* 2011
yRP1919	*dcp1*Δ Not5	*Mat alpha trp1 leu2-3, 112 cup1::LEU2/PGK1pG/MFA2pG ura3-52 dcp1::URA3 NOT5-GFP(NEO)*	N		Sheth *et al* 2003, Teixeira *et al* 2007
yRP3083	*dcp1*Δ Scd6	*Mat alpha leu2, ura3, his3, met15, dcp1::URA3 SCD6::GFP(HIS3MX6)*	N	Compete binding sites on Dcp2 with Edc3. Because Edc3 is highly concentrated, Scd6 partitioning can be very poor.	Rajyaguru *et al* 2012
yRP3142	*dcp1*Δ Brf1	*Mat alpha leu2, ura3, his3, met15, dcp1::URA3 BFR1::GFP(HIS3MX6)*	N	Reported to localize to P bodies after 50min - glucose. Might be stress specific	Simpson *et al* 2014
yRP3144	*dcp1*Δ Dcs1	*Mat alpha leu2, ura3, his3, met15, dcp1::URA3 DCS1::GFP(HIS3MX6)*	N	P body localization is not shown by microscope	Malys *et al* 2006
yRP3145	*dcp1*Δ Dcs2	*Mat alpha leu2, ura3, his3, met15, dcp1::URA3 DCS2::GFP(HIS3MX6)*	N	Dcs2 is reported to locate in P bodies as cells progressed into diauxie. We only analyzed log-phase cells.	Malys *et al* 2006
yRP3139	*dcp1*Δ Edc2	*Mat alpha leu2, ura3, his3, met15, dcp1::URA3 EDC2::GFP(HIS3MX6)*	N	A subset of it is reported to localize to P bodies under glucose starvation or del_Xrn1 strains. Maybe stress specific.	Neef *et al* 2009
yRP3141	*dcp1*Δ Rbp4	*Mat alpha leu2, ura3, his3, met15, dcp1::URA3 RBP4::GFP(HIS3MX6)*	N	P body localization increased after 4h starvation (lacking both glucose and amino acid) and increased more after 24 stravation. May be stress specific.	Lotan *et al* 2005
yRP3153	*dcp1*Δ Rbp7	*Mat alpha leu2, ura3, his3, met15, dcp1::URA3 RBP7::GFP(HIS3MX6)*	N	Rpb7 co-localizes with Dcp2 after long starvation. May be stress specific	Lotan *et al* 2007
	*dcp1*Δ Sup45		N		Buchan *et al* 2008

Table S3. Plasmids used in this study

Plasmid name	description	makers	N-terminal tag	C-terminal tag	
Dcp2 FL	carrying the *DCP2* promoter, a sequence encoding full length Dcp2 (1-970) - GFP and the *ADH1* terminator	amp+, -URA		GFP	
Dcp2 ΔN	carrying the *DCP2* promoter, a sequence encoding Dcp2 (243-970) - GFP and the *ADH1* terminator	amp+, -URA		GFP	
Dcp2 ΔH1	carrying the *DCP2* promoter, a sequence encoding Dcp2 (1-970) L255A - GFP and the *ADH1* terminator	amp+, -URA		GFP	
Dcp2 300	carrying the *DCP2* promoter, a sequence encoding Dcp2 (1-300) - GFP and the *ADH1* terminator	amp+, -URA		GFP	
Dcp2 300 ΔH1	carrying the *DCP2* promoter, a sequence encoding Dcp2 (1-300) L255A - GFP and the *ADH1* terminator	amp+, -URA		GFP	
Dcp2 300 AAAA	carrying the *DCP2* promoter, a sequence encoding Dcp2 (1-300) R170A K212A K216A R229A - GFP and the *ADH1* terminator	amp+, -URA		GFP	
Dcp2 300 ADDA	carrying the *DCP2* promoter, a sequence encoding Dcp2 (1-300) R170A K212D K216D R229A - GFP and the *ADH1* terminator	amp+, -URA		GFP	
Dcp2 ΔH1 WD	carrying the *DCP2* promoter, a sequence encoding Dcp2 (1-970) L255A W50A D54A-GFP and the *ADH1* terminator	amp+, -URA		GFP	
Dcp2C Δ5H	carrying the *DCP2* promoter, a sequence encoding Dcp2 (327-970) X440-450A X489-500A, X701-708A, X827-831A, X935-938A - GFP and the *ADH1* terminator	amp+, -URA		GFP	five Edc3 binding regions 440-450, 489-500, 701-708, 827-831, 935-938 were mutated to alanine
Dcp2 ΔH1 Δ5H	carrying the *DCP2* promoter, a sequence encoding Dcp2 (1-970) L255A X440-450A X489-500A, X701-708A, X827-831A, X935-938A - GFP and the *ADH1* terminator	amp+, -URA		GFP	five Edc3 binding regions 440-450, 489-500, 701-708, 827-831, 935-938 were mutated to alanine
N-Dcp2	carrying the *DCP2* promoter, a sequence encoding GFP - Dcp2 (1-970) and the *ADH1* terminator	amp+, -URA	GFP		
Edc3	carrying the *EDC3* promoter, a sequence encoding Edc3-mCherry and the *EDC3* terminator	amp+, -LYS		mCherry	
Edc3	carrying the *EDC3* promoter, a sequence encoding Edc3-mCherry and the *EDC3* terminator	amp+, -TRP		mCherry	

yRP3148	*dcp1*Δ Smy2	*Mat a leu2, ura3, his3, met15, dcp1::URA3 SMY2::GFP(HIS3MX6)*	N	Localization of P body was found using transfected plasmid. May be partition into P bodies when overexpressed.	Georgiev *et al* 2007
yRP3147	*dcp1*Δ Tis11	*Mat a leu2, ura3, his3, met15, dcp1::URA3 TIS11::GFP(HIS3MX6)*	N	Binds to 3'UTR of specific mRNAs and partition into P bodies when expressing on plasmid. May be overexpressed, or the specific mRNAs are not in P bodies under our experimental conditions.	Pedro-Segura *et al* 2008
yRP3138	*dcp1*Δ Pby1	*Mat a leu2, ura3, his3, met15, dcp1::URA3 PBY1::GFP(HIS3MX6)*	N	Pby1 is reported to interact with Dcp1. Lacking the factor recruiting Pby1 into P bodies in dcp1Δ strain.	Sweet *et al* 2007
RESGEN	WT Dcp2	MATa his3Δ leu2Δ met15Δ ura3Δ DCP2::GFP(HIS3MX6)	Y		Sheth *et al* 2003
RESGEN	WT Edc3	MATa his3Δ leu2Δ met15Δ ura3Δ EDC3::GFP(HIS3MX6)	Y		Kshirsagar *et al* 2004
RESGEN	WT Pat1	MATa his3Δ leu2Δ met15Δ ura3Δ PAT1::GFP(HIS3MX6)	Y		Sheth *et al* 2003
RESGEN	WT Xrn1	MATa his3Δ leu2Δ met15Δ ura3Δ XRN1::GFP(HIS3MX6)	Y		Sheth *et al* 2003
RESGEN	WT Lsm1	MATa his3Δ leu2Δ met15Δ ura3Δ LSM1::GFP(HIS3MX6)	Y		Sheth *et al* 2003
RESGEN	WT Upf1	MATa his3Δ leu2Δ met15Δ ura3Δ UPF1::GFP(HIS3MX6)	Y		Sheth *et al* 2006
RESGEN	WT Dhh1	MATa his3Δ leu2Δ met15Δ ura3Δ DHH1::GFP(HIS3MX6)	Y		Sheth *et al* 2003
RESGEN	WT Pop2	MATa his3Δ leu2Δ met15Δ ura3Δ POP2::GFP(HIS3MX6)	N		Sheth *et al* 2003, Teixeira *et al* 2007
RESGEN	WT Upf3	MATa his3Δ leu2Δ met15Δ ura3Δ UPF1::GFP(HIS3MX6)	N		Sheth *et al* 2006
RESGEN	WT Not2	MATa his3Δ leu2Δ met15Δ ura3Δ NOT2::GFP(HIS3MX6)	N		Sheth *et al* 2003, Teixeira *et al* 2007
RESGEN	WT Upf2	MATa his3Δ leu2Δ met15Δ ura3Δ UPF2::GFP(HIS3MX6)	N		Sheth *et al* 2006
RESGEN	WT CCR4	MATa his3Δ leu2Δ met15Δ ura3Δ CCR4::GFP(HIS3MX6)	N		Sheth *et al* 2003, Teixeira *et al* 2007
RESGEN	WT Hek2	MATa his3Δ leu2Δ met15Δ ura3Δ HEK2::GFP(HIS3MX6)	Y		Mitchell *et al* 2013
RESGEN	WT Sbp1	MATa his3Δ leu2Δ met15Δ ura3Δ SBP1::GFP(HIS3MX6)	Y		Mitchell et al 2013
RESGEN	WT Edc1	MATa his3Δ leu2Δ met15Δ ura3Δ EDC1::GFP(HIS3MX6)	N		Neef *et al* 2009
RESGEN	WT Bre5	MATa his3Δ leu2Δ met15Δ ura3Δ BRE5::GFP(HIS3MX6)	N		Mitchell *et al* 2013
RESGEN	*WT* Psp2	MATa his3Δ leu2Δ met15Δ ura3Δ PSP2::GFP(HIS3MX6)	N		Mitchell *et al* 2013
RESGEN	WT Eap1	MATa his3Δ leu2Δ met15Δ ura3Δ EAP1::GFP(HIS3MX6)	N		Buchan *et al* 2008
RESGEN	WT Ssd1	MATa his3Δ leu2Δ met15Δ ura3Δ SSD1::GFP(HIS3MX6)	N		Kurischko *et al* 2011
RESGEN	WT Not5	MATa his3Δ leu2Δ met15Δ ura3Δ NOT5::GFP(HIS3MX6)	N		Sheth *et al* 2003, Teixeira *et al* 2007
RESGEN	WT Scd6	MATa his3Δ leu2Δ met15Δ ura3Δ SCD6::GFP(HIS3MX6)	N		Rajyaguru *et al* 2012
RESGEN	WT Brf1	MATa his3Δ leu2Δ met15Δ ura3Δ BRF1::GFP(HIS3MX6)	N		Simpson *et al* 2014
RESGEN	WT Dcs1	MATa his3Δ leu2Δ met15Δ ura3Δ DCS1::GFP(HIS3MX6)	N		Malys *et al* 2006
RESGEN	WT Dcs2	MATa his3Δ leu2Δ met15Δ ura3Δ DCS2::GFP(HIS3MX6)	N		Malys *et al* 2006
RESGEN	WT Edc2	MATa his3Δ leu2Δ met15Δ ura3Δ EDC2::GFP(HIS3MX6)	N		Neef *et al* 2009
RESGEN	WT Rbp4	MATa his3Δ leu2Δ met15Δ ura3Δ RPB4::GFP(HIS3MX6)	N		Lotan *et al* 2005
RESGEN	WT Rbp7	MATa his3Δ leu2Δ met15Δ ura3Δ RBP7::GFP(HIS3MX6)	N		Lotan *et al* 2007
RESGEN	WT Sup45	MATa his3Δ leu2Δ met15Δ ura3Δ RBP7::GFP(HIS3MX6)	N		Buchan *et al* 2008
RESGEN	WT Smy2	MATa his3Δ leu2Δ met15Δ ura3Δ SMY2::GFP(HIS3MX6)	N		Georgiev *et al* 2007
RESGEN	WT Tis11	MATa his3Δ leu2Δ met15Δ ura3Δ TIS11::GFP(HIS3MX6)	N		Pedro-Segura *et al* 2008
RESGEN	WT Pby1	MATa his3Δ leu2Δ met15Δ ura3Δ PBY1::GFP(HIS3MX6)	Y		Sweet *et al* 2007
RESGEN	WT Dcp1	MATa his3Δ leu2Δ met15Δ ura3Δ DCP1::GFP(HIS3MX6)	Y		

Table S4. Multivalent intermolecular Protein-Protein and Protein-RNA interactions among P body proteins

	protein protein interactions (no. of interactions)	Protein-RNA interactions	Total valency	References
Dcp2	Edc3 + Pat1(10 in total), Dhh1, Edc1	1	13	Harigaya et al., 2010; Decker et al., 2007; Nissan et al., 2010; Dunckley et al., 2001; Charenton et al., 2017
Edc3	Dcp2, Edc3, Dhh1, Upf1, Pat1	>=1	>=6	Harigay et al., 2010; Decker et al., 2007, Swisher et al., 2011; Pilkington and Parker, 2008
Pat1	Pat1, Dcp2/Xrn1 (same site), Dhh1, Edc3, Lsm1-7, Upf1	1	8	Nissan et al., 2010; Swisher et al., 2011; Pilkington and Parker, 2008
Xrn1	Pat1	1	2	Nissan et al., 2010
Lsm1-7	Pat1, Lsm4 Q/N domain (>=1)	1+1	4	Decker et al., 2007; Sharif and Conti, 2013;
Upf1	Pat1, Edc3, Upf2	1	4	Swisher et al., 2011
Dhh1	Pat1/Edc3 (same site), Dcp2, Pop2, Eap1	>=1	5	Nissan et al., 2010; Decker et al., 2007; Blewett and Goldstrohm, 2011; Coller et al., 2001
Pop2/CCR4/Not2	Dhh1	1	2	Coller et al., 2001; Basquin et al., 2012;
Upf3	Upf2	1	2	He et al., 1997
Upf2	Upf1	1	2	Swisher et al., 2011
Hek2		>=1	>=1	Irie et al., 2002
Sbp1		>=1	>=1	Mitchell et al., 2013
Edc1	Dcp2	2	2	Schwartz et al., 2003
Bre5	Bre5	1	2	Li et al., 2005
Psp2		1	1	Mitchell et al., 2013
Eap1	Dhh1	1	2	Blewett and Goldstrohm., 2011
Ssd1		1	1	Uesono et al., 1997

1) Did not consider high-throughput studies
2) Unclear if interactions between Pat1 and Upf1 is direct. Demonstrated by two-hybrid assays.
3) Lsm4 valency is unclear
4) Interactions between Dhh1 and Pop2, Dhh1 and Eap1 were demonstrated by Co-IP, unclear if the interactions are direct
5) Hek2 has 3 RNA binding KH domains, but whether all of them interact with RNA is unclear
6) Sbp1 has 2 RRM domains, not sure if they all interact with RNA.